$^{87}Sr/^{86}Sr$ and trace element mapping of geosphere-hydrosphere-biosphere interactions: A case study in Ireland

SASKIA E. RYAN[1]*, CHRISTOPHE SNOECK[2,3], QUENTIN G. CROWLEY[1] & MICHAEL G. BABECHUK[1, 4]

[1] Department of Geology, School of Natural Sciences, Trinity College, Dublin 2, Ireland (*correspondence: ryans22@tcd.ie)

[2] Research Laboratory for Archaeology and the History of Art, University of Oxford, Dyson Perrins Building, South Parks Rd, Oxford, OX1 3QY, UK.

[3] Research Unit: Analytical, Environmental & Geo-Chemistry, Dept. of Chemistry, Vrije Universiteit Brussel, ESSC-WE-VUB, Pleinlaan 2, 1050 Brussels, Belgium.

[4] Department of Earth Sciences, Memorial University of Newfoundland, St. John's, Canada.

Keywords: strontium isotopes, rare earth elements and yttrium (REE+Y), biosphere, geographical discrimination, biological availability.

Abbreviations:

REE+Y = Rare earth elements and Y

LREE = Light rare earth element (from La to Eu)

HREE = Heavy rare earth element (from Gd to Lu)

BASr = Biologically available strontium

BAC = Biological absorption coefficient

MUQ = Mud from Queensland (trace element normalisation)

[Sr] = Sr concentration

Abstract

Geochemical mapping of biosphere variation has wide application to geological, environmental, forensic and archaeological research. The extent to which trace elements may be used to complement strontium isotopes ($^{87}Sr/^{86}Sr$) for biosphere characterisation is unclear and uncertainties exist regarding the most suitable sample media for this purpose. Here, the variation in $^{87}Sr/^{86}Sr$ and trace elements, with focus on the rare earth elements and yttrium (REE+Y), are measured in soil leachates, vegetation and streamwaters. These independent tracers are employed to define geochemical reservoirs and quantify soil-plant-water

interactions in a geologically diverse and archaeologically significant area of Ireland, County (Co.) Meath. This integrated isotope and element approach produces the first combined dataset for this temperate environment.

Biological absorption coefficients (BAC) are used to assess bio-uptake of selected elements. The REE+Y exhibited greatest utility in revealing soil parameter controls on bio-uptake, such as reduced availability from preferential retention of Ce on Mn/Fe-hydr(oxide) surfaces, as well as revealing a preferential uptake of Y relative to HREE. High Y/Ho ratios (65.3-465.1) are exhibited in ash tree samples (*Fraxinus excelsior L.*), regardless of geological setting, indicating a potential species-specific preference. However, aerial portions of ash trees do not directly reflect the REE in the bioavailable portion of the soil, indicating selectivity from the soil reservoir or fractionation during plant uptake and/or intra-plant distribution. Streamwater REE patterns have a consistent and seawater-like pattern probably inherited from marine carbonate bedrock, surficial marine carbonate-derived till, agricultural fertiliser or a combination of all three, and thus were not site lithology diagnostic. By contrast, distinct variation in sources of $^{87}Sr/^{86}Sr$ to streamwaters is evident and reflects small-scale differences in underlying bedrock.

The $^{87}Sr/^{86}Sr$ range of vegetation for the study area is 0.7081 to 0.7130. Soil and streamwater samples collected at proximal locations to the vegetation demonstrated a range of 0.7086 to 0.7133 for soil leachates and 0.7081 to 0.7107 for streamwaters. Statistically significant ($p<0.05$) differences between the spatial distribution of $^{87}Sr/^{86}Sr$ in plants and certain underlying bedrock/Quaternary sediment were identified, even in a region without an extreme range in $^{87}Sr/^{86}Sr$ values. Careful selection of appropriate soil leaching protocols is necessary for an informative estimate of the natural ranges that exist within the pedosphere, supporting the notion that plant material is the most suitable sample medium for mapping bioavailable Sr. The high degree of spatial variability in $^{87}Sr/^{86}Sr$ and differences between reservoirs can only be accurately represented by relatively high-density sampling of plants. These data complement both national and European-wide initiatives to produce large-scale $^{87}Sr/^{86}Sr$ biosphere maps.

1 Introduction

Mapping geochemical variations of local biosphere values has wide application to geological, environmental, archaeological, forensic and food authenticity research (eg. Bataille and Bowen, 2012; Beard and Johnson, 2000a; Bentley, 2006; Capo et al., 1998; Evans et al., 2012, 2010; Laffoon, 2012; Laffoon et al., 2017, 2012; Maurer et al., 2012; Montgomery, 2010; Price, 2015; Sealy et al., 1991; Sillen and Kavanagh, 1982; Vinciguerra et al., 2016). Spatially defined biosphere geochemical maps can elucidate elemental and isotope reservoirs and their interactions at the Earth's surface. Strontium isotope ratios ($^{87}Sr/^{86}Sr$) have been used extensively as a geographical discriminant and as a geochemical tracer of weathering processes, in some cases, in combination with rare earth elements (REE+Y) and other trace elements (Aubert et al., 2001; Lagad et al., 2017; Tricca et al., 1999). Independently, the REE have emerged as a powerful tracer of water source, water mixing, and aqueous processes (e.g. Noack et al., 2014; Pourret et al., 2010; Tweed et al., 2006), in addition to chemical weathering process and soil formation (Babechuk et al., 2014; Condie, 1991; Hu et al., 2006; Laveuf and Cornu, 2009; Nesbitt, 1979), and studies of plant material (Brioschi et al., 2013; Miao et al., 2011; Squadrone et al., 2017; Thomas et al., 2014; Tyler, 2004).

Within the last 15 years there have been numerous large scale Sr isoscapes developed using biosphere samples (e.g. Åberg et al. 1998; Bentley & Knipper 2005; Evans et al. 2009; Evans et al. 2010; Frei & Frei 2011; Frei & Frei 2013; Hartman & Richards 2014; Hedman et al. 2009; Hodell et al. 2004; Knudson & Torres-Rouff 2009; Kootker et al. 2016; Laffoon et al. 2012; Nafplioti 2011; Porder et al. 2003; Price and Naumann, 2015; Sjögren et al. 2009; Thornton 2011; Voerkelius et al. 2010; Willmes et al. 2014; Zitek et al. 2015), however none of these has specifically dealt with detailed Sr isoscapes in Ireland. At present, there are relatively few published data dealing with spatial variation of $^{87}Sr/^{86}Sr$ in the Irish biosphere using environmental samples (Cahill Wilson and Standish, 2016; Knudson et al., 2012; Snoeck et al., 2016; Voerkelius et al., 2010), despite the fact that $^{87}Sr/^{86}Sr$ are commonplace as a provenance tool applied to archaeological studies (e.g. Montgomery, Evans, and Chenery, 2006; Wallace et al., 2010; Montgomery and Grimes, 2010; Montgomery et al., 2014; Kador et al., 2014; Sheridan et al., 2013). For $^{87}Sr/^{86}Sr$ to be applicable to Irish case studies, a baseline reference dataset is imperative, especially in areas of archaeological significance. The context of this study, Co. Meath, is a storehouse of archaeology; the Hill of Tara, the Norman settlement of Trim, the Megalithic sites of the Boyne Valley, Loughcrew and many other sites

have been extensively studied but await extended investigation using environmental $^{87}Sr/^{86}Sr$ isotope data. This study provides baseline $^{87}Sr/^{86}Sr$ data for use in future archaeological studies in this region and in cases where ancient human mobility associated with the locality is in question.

This research aims to geochemically characterise the degree of biosphere variation between specific element reservoirs and investigate geosphere-biosphere-hydrosphere interactions using $^{87}Sr/^{86}Sr$ and REE+Y proxies. To document the spatial variability in geochemical signatures, three sample media were used; vegetation, streamwaters and surface soils. A sampling density of >1 sample per 20km^2 was used here to examine spatial geochemical heterogeneity, with implications for $^{87}Sr/^{86}Sr$ values inferred from larger-scale biosphere maps. The REE+Y are naturally present in soils and are important in calculating material fluxes/geochemical budgets within catchments (Aubert et al., 2002a) and due to the REE+Y variability between geological and hydrological environments, smaller-scale studies on REE+Y systematics are of significant merit (Noack et al., 2014) and are key to interpreting regional natural REE+Y variability. Their abundances are used here to elucidate the origin and mobility behaviour of lanthanides and yttrium in soil-plant-water systems, with emphasis on possible substrate-vegetation fractionation. The distribution of REE+Y from substrate into the dissolved load of streams is also examined to test the degree of inheritance from rock-soil-water interactions.

1.1 Estimating element bioavailability in soil

The $^{87}Sr/^{86}Sr$ of a particular bedrock depends on both its age and geochemical composition (Faure and Powell, 1972). Whilst it is assumed on a larger scale that biosphere values will generally correspond with major lithological boundaries (Beard and Johnson, 2000), this is not always the case. Biosphere $^{87}Sr/^{86}Sr$ ranges do not usually directly resemble whole-rock values because bioavailable Sr originates from rock-weathering products, non-local glaciogenic material and atmospheric and anthropogenic inputs in varying combinations, often with distinctive isotopic fingerprints (Ericson, 1985). Furthermore, plants preferentially source certain elements from soils that have been progressively enriched in more stable minerals, with respect to underlying geology due to preferential weathering (Bain and Bacon, 1994). Although geochemical vectoring using plants is relatively commonplace in economic geology when spatially defining ore bodies or geochemical anomalies (Brooks, 1972; Dunn, 2007), the

relationship between the trace element chemistry of plants and underlying soil, Quaternary deposits and bedrock is not always clear (Bentley, 2006; Capo et al., 1998).

In terms of bedrock and mineral composition, Sr is likely to occur in elevated concentrations in intermediate igneous rocks, calcareous sediments and sulphate rich deposits and its distribution within minerals is most strongly controlled by Ca (Kabata-Pendias, 2001). Sorption and desorption processes such as precipitation, complexation, and ion exchange largely control the behaviour of Sr in soils which in turn are controlled by pH, ionic strength, solution speciation, mineral composition, organic matter, biological organisms, and temperature (Kabata-Pendias, 2001). Strontium ions can sorb as hydrated ions on iron oxides and clay minerals (Sahai et al., 2000) and therefore argillaceous sediments tend to be enriched in Sr. However, generally, Sr is easily mobilised and readily exchangeable (Bunker et al., 2000). Organic matter in soils can strongly fix Sr and so it too has a major effect on the mobility of Sr from soils into groundwater (Wiche et al., 2017). The mean Sr concentration of soils across the United States of America, for instance, is on average around 120 mg/kg (Shacklette and Boerngen, 1984), whereas for Ireland this is estimated to be approximately 80 mg/kg for bulk soils and 30 mg/kg for quasi-bulk soils (Young et al., 2016; Young and Donald, 2013). High concentrations of Sr are expected in loamy, calcareous or industrial soils whilst soils that have low organic matter and clay content, such as more sandy soils, generally have lower Sr content (Kabata-Pendias, 2001).

The REE are another useful tracer of element cycling at the soil-plant interface. In contrast to Sr content, ultramafic igneous and calcareous rocks have the lowest concentrations of REE. In soils, REE can be mobile and preferential mobility between the light REE (LREE) and heavy REE (HREE) or inter-element fractionation within these groups reflects a complex interplay between host mineralogy, complexation behaviour (e.g., available carbonate ions or organic ligands), available pedogenic mineral surfaces, which are in turn controlled by soil parameters such as Eh and pH (e.g. Hu et al., 2006; Kabata-Pendias, 2001; Khan et al., 2017; Laveuf and Cornu, 2009; Vázquez Vázquez et al., 2016). Nevertheless, specific soil parameters can be elucidated from the REE, such redox parameters revealed by the contrasting geochemical behaviour of Ce(III) vs. Ce(IV) leading to separation of Ce from the strictly trivalent REE and indicating oxic conditions that support the formation of Fe/Mn-oxy(hydroxides) (Aide and Aide, 2012; Miao et al., 2008; Pédrot et al., 2015a; Wang and Liang, 2014; Wyttenbach et al., 1998). Other studies have found utility in examining inter-element fractionation that reflects

differences in complexation behaviour, such as the fractionation of Y and Ho (Thompson et al., 2013; Babechuk et al., 2015), which have highly contrasting affinity for complexation due to their differences in orbital chemistry, but are otherwise tightly coupled in the absence of ligands (Bau, 1996). Although the overall budget of REE available in soils in parent lithology and mineralogy specific, most parent materials have REE concentrations ranging from 0.1 to 100 mg/kg (Aide and Aide, 2012).

The bulk concentration of trace elements and Sr in soils reside in the leach-resistant detritus rather than the leachable pool (Sholkovitz et al., 1994), but it is the latter that is immediately bioavailable for plants. The REE concentrations of soil pore fluids and soil leaches are generally controlled by the solubility of REE-bearing minerals and therefore do not directly reflect the REE concentrations of the bulk soil (Braun et al., 1998). Nevertheless, leaching of soils in order to estimate the bioavailability of REE has been extensively studied – see Hu et al., (2006) and references for multiple examples contained therein. To empirically assess the bioavailability of Sr and the REE in soils, a common strategy is the use of leaching experiments. There is some debate about how successfully leaching experiments replicate the bioavailability of elements within a natural system because REE and Sr in soil can be found in numerous soil fractions and can thus be defined by the chosen extraction method. The key fractions are: the water-soluble, the exchangeable, the carbonate, the amorphous oxides, the manganese oxide bound (Fe/Mn-oxy(hydroxides)), the organically bound, the crystalline oxide, and the residual fraction. The water soluble and/or exchangeable fractions are commonly targeted for studying biogeochemical cycling (e.g. Drouet et al., 2007; Fang et al., 2007; Frei et al., 2009; Leybourne and Johannesson, 2008; Loell et al., 2011; Miller et al., 1993; Poszwa et al., 2000; Tyler, 2004)

1.2 REE+Y translocation to plants

Examining the biogeochemical relationship between soil and plants enables distinction of key geochemical anomalies and their significance for element transfer between these environmental media. The potential effect of REE+Y on plant growth and their mechanisms for entering into biomass is of growing interest, particularly the uptake, distribution and accumulation of REE+Y in plants (Wyttenbach et al. 1998; Tyler 2004; Tyler & Olsson 2005; Brioschi et al. 2013; Wen et al. 2001; Fu et al. 2001; Censi et al. 2014; Miao et al. 2008; Miao et al. 2011; Lima e Cunha et al. 2014; Ding et al. 2006; Hu et al. 2006). Despite this, the REE+Y

content of wild-growing plants in natural ecosystems is much less studied. Both organic and inorganic processes play a role in the uptake of elements by plant roots from the rhizosphere, but generally, plant REE+Y are controlled by the type of soils on which they grow and the plant species in question (Fu et al., 2001; Miekeley et al., 1994). The biomass signature is an end-member in a mixing system of soil/water/rock. Direct rhizospheric acidification of the mineral particles (mostly Fe/Mn-oxy(hydroxide) and clay particles) is the suggested physicochemical process by which REE+Y are made soluble and available for uptake by plants (Brioschi et al., 2013). In terms of the correspondence between soils and plant REE+Y signatures, complex relationships between concentrations in these media have been demonstrated (Laul et al. 1979; Robinson et al. 1958; Tyler and Olsson 2005). This complexity is due to differing REE+Y concentrations within soil horizons and species-dependent absorption capabilities (Lima e Cunha et al., 2014). The Biological Absorption Coefficient (BAC), the ratio of an element concentration in a plant to that in the soil, or soil fraction, can be used to quantify and predict the relative difference in bioavailability of elements in the soil-plant system (Ebong et al., 2007).

1.3 REE+Y in the hydrological system

Examining the relationship between REE+Y characteristics of soil/plant and small streams is of growing interest for understanding element cycling (Aubert et al., 2002b; Brioschi et al., 2013; Cidu et al., 2013; Miao et al., 2008). The dissolved REE+Y composition of local streams is controlled to some degree by the local catchment geology and weathering conditions, providing a snapshot of the flux to the hydrosphere. However, in any given drainage basin, physio-chemical parameters such as pH, dissolved organic carbon (DOC) concentration, aquatic chemistry processes, weathering of individual mineral phases and land use can also influence the measured REE+Y chemistry of river waters (Byrne and Sholkovitz, 1996; Chudaev et al., 2016; Deberdt et al., 2002; Elderfield et al., 1990; Lawrence and Kamber, 2006; Matsunaga et al., 2015; Noack et al., 2014; Pédrot et al., 2015a; Tricca et al., 1999), in addition to REE complexation with organic and inorganic ligands (Johannesson et al., 1999; Johannesson and Zhou, 1999; Millero, 1992).

The REE+Y patterns of many large rivers are relatively flat when normalised to shale (Elderfield et al., 1990), demonstrating their similar pattern with the average upper continental crust (often approximated with shale composites) and assumed to be a broad representation of

the original REE+Y source (Piper and Bau, 2013). In such cases, this similarity indicates that the relative abundances of the REE+Y are not markedly fractionated during weathering and aqueous transport. However, at a finer scale the REE+Y patterns of smaller streams or rivers often broadly reflect the predominant lithology in the catchments and allow these elements to be exploited as a tracer of water source and mixing (Lawrence et al., 2006a, 2006b; Sadeghi et al., 2013; Zhang et al., 2003). Groundwater and river/streamwater associated with marine-derived carbonate-rich catchments often exhibit LREE depleted patterns that resemble seawater (e.g. Elderfield et al. 1990; Smedley 1991; Johannesson & Lyons 1994; Sholkovitz 1995; Johannesson et al. 1999; Johannesson & Hendry 2000; Leybourne et al. 2000; Négrel et al. 2000). In this study, REE+Y in immature streams from small drainage catchments in Co. Meath were measured to determine the origin and behaviour of REE+Y and better understand the connection between the dissolved load REE+Y distribution patterns with the principle underlying lithologies and overlying sediments.

1.4 Study site

Co. Meath is located in the east midlands of Ireland between 53° 21' W and 53° 55’ W and 6° 12' N and 7° 20' N (Fig. 1). The field area of Co. Meath and proximal surrounding areas, covers approximately 2,500km^2 and has a typical temperate oceanic climate that is subject to south-westerly prevailing winds. Despite some small-scale variation in temperature and rainfall throughout the area, it can essentially be classified as a single bio-climatic zone. The region has a relatively flat topography due to glacial erosion and an extensive blanket of glacial sediments. Aside from a small area in northwest Co. Meath, all rivers drain eastwards towards the Irish Sea, including, Dee, Boyne and Nanny (Finch et al., 1983).

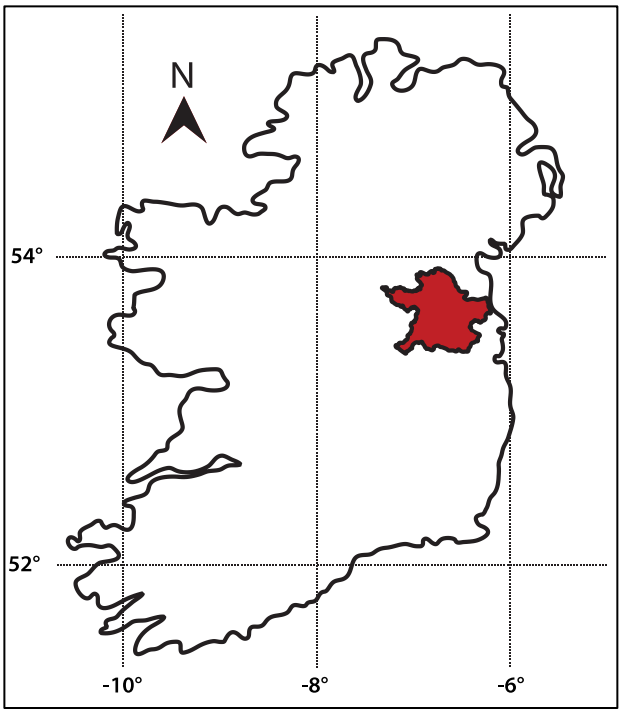

Figure 1. Map of the study site - Co. Meath, Ireland, indicated by the red highlighted region.

The study area encompasses a high degree of bedrock variability over a relatively small area. The bedrock geology consists largely of marine-derived sediments, primarily basinal facies and argillaceous and cherty limestone and shale that are late Palaeozoic in age (Geological Survey of Ireland, 2009). Bedrock can be grouped into three dominant rock types: (1) Ordovician and Silurian lithologies, (2) Upper Carboniferous shale and (3) Carboniferous limestone (Finch et al., 1983). Further details on the geological history and formation of the regional bedrock can be found in Clarke et al., (2007), McConnell et al., (2001) and Meehan and Warren, (1999). Four distinct bedrock units were selected as comparative sites, from which a plant, soil and streamwater sample was collected: the bedrock units were, Ordovician-Silurian shale, Permian sandstone, Carboniferous limestone and a small outcrop of Devonian basalt.

The bedrock geology is variably covered by Quaternary sediments, mostly deposited during the Pleistocene (McCabe, 2007). These sediments include till, fluvioglacial gravels and sands of varying provenance including local bedrock as well as more distal clasts from the Irish Sea and Scandinavia (McCabe, 2007). Owing to the contribution from this source, the bioavailable $^{87}Sr/^{86}Sr$ may not directly reflect bedrock Sr compositions and therefore, the underlying bedrock geology, is not a straightforward proxy for bioavailable Sr. Here, the extent to which distinct geological units can be characterised over the study area by regionally unique $^{87}Sr/^{86}Sr$ values or REE patterns is examined.

2 Materials and Methods

2.1 Sampling strategy

Sampling density and location were organised around distribution of principal chrono-stratigraphic units on the 1:500 000 geological map of Co. Meath (Geological Survey of Ireland, 2016). A plant sample was collected at each site and at four additional representative sites, selected on their distinct bedrock and/or Quaternary deposits, surface soils and streamwater were collected in addition to the plant samples. To avoid contamination by modern day fertilisers, samples were taken from forested, non-agricultural land. The sampling methods followed in this study were adapted from those outlined by the British Geological Survey (BGS) (Johnson et al., 2005; Smyth, 2007) and adhere to the proposed standardised field methods specifically for $^{87}Sr/^{86}Sr$ (Grimstead et al., 2017).

Vegetation samples consisted mainly of grass, fern, heather, ash and other twiggy deciduous material (woody twigs of mature shrubby trees). All plant samples for which REE+Y concentrations were measured are of the species ash, *Fraxinus excelsior L.* and the terminal branches were sampled.

Soil was taken at proximal locations to the vegetation from the surface A-horizon (5-20cm). Soil mineral particles close to the plant roots (in the rhizospheric zone) are more likely to be the main REE+Y source for plants and it is for this reason that the upper horizon of the soil was leached in this study. Moreover, ash trees have an abundance of surface roots with intensive superficial root systems that are far-reaching and dominate the upper 0–5 cm of the soil profile (Rust and Savill, 2000). Soil samples were collected from five points at the corners and the centre of a 20 x 20 m square, combined to form a composite sample of ~1 kg. The bedrock and/or Quaternary substrate on which the collected soils developed is defined in Table 1.

Streamwater was collected from the active portions of small first- and second-order catchment locations that integrate material from an area of no more than a few square kilometres. The ‘clean hands, dirty hands’ sampling procedure (U.S. EPA, 1996) was adopted. Sites were at least 50 m upstream of roads, reducing the risk of anthropogenic runoff contamination. Water samples were collected in acid-cleaned polypropylene bottles filtered immediately by 0.45 μm

pore size Millipore HDPE membranes, acidified with ultrapure HNO_3 (to 1% v/v) and stored refrigerated (~4°C) until analysis. The fraction that passed through this filter is considered as the 'dissolved load' and is known to consist of colloids less than 0.45 μm in addition to the truly dissolved fraction. Both the syringe and water filter were rinsed several times in the streamwater and the first portion of the filtration was discarded to clean the membrane.

2.2 Sample preparation and digestion

Sample preparation and digestion were carried out in two different laboratories: in the Geochemistry Laboratory at Trinity College Dublin (TCD), Ireland and in the G-Time Laboratory at the Université Libre de Bruxelles (ULB), Belgium. All reagents were prepared using triple-distilled HNO_3 and ultrapure water. At TCD, plant samples were placed in quartz glass crucibles and ashed in a furnace at 600°C for 8 hours. A 0.1 g aliquot of each sample was digested in 1mL ultrapure concentrated HNO_3 for at least 1 hour before evaporating to dryness and being redissolved in 2 mL 2 mol/L HNO_3.

To separate the water soluble and the exchangeable/labile soil fractions of the soil and hence characterise the origin and bioavailability of Sr and REE+Y that can be desorbed by natural solutions in the soil, separate leaching experiments were performed using either ultra-pure H_2O (Maurer et al., 2012; Pierson-Wickmann et al., 2009) or 1 mol/L NH_4NO_3 (DIN:ISO (German Institute for Standardization) ISO (International Organization for Standardization); Loell et al. 2011; Willmes et al. 2014; Zhai et al., 1999). Using these reagents provided a best estimate of (1) the cations available for plants via ion-exchange in the soil (NH_4NO_3), and (2) the cations leachable with water flowing through the soil (ultra-pure H_2O). These solutions do not extract elements bound to organics (Caporale and Violante, 2016). According to Pearcy et al. (2000), the particular salt solution chosen does not significantly affect the amount of ions extracted, as in any case, nearly all exchangeable cations are released into solution. An extensive sequential leach is therefore not generally necessary. The soil samples were dried in an oven for 48 hours at 60°C. Two 1 g aliquots were used for the two different leaching methods. The first method used 2.5 mL of 1 mol/L NH_4NO_3 and was constantly agitated for 8 hours. The second leaching method used 10 mL of MilliQ H_2O and was constantly agitated for 24 hours. Extractions were conducted at room temperature. All samples were then centrifuged at 3000 rpm for 20 minutes. The supernatant fluid was extracted and evaporated to dryness and then redissolved in 2 mL 2

mol/L HNO_3. To prepare the streamwaters for chemical analysis, 15 mL of sample was evaporated in PMP beakers to which 1 mL of concentrated HNO_3 was subsequently added and left to react for approximately 12 hours in order to attack organics and convert to nitrate for loading on the column. The concentrated HNO_3 was then evaporated and the sample was redissolved in 2 mL of 2 mol/L HNO_3.

At ULB, additional plant samples were placed in porcelain crucibles and ashed by step heating in a muffle furnace at 650 ºC. The entire acid digestion process and subsequent Sr purification was carried out under a class 100 laminar flow hood in a class 1000 clean room (Université Libre de Bruxelles, Belgium). 50 mg of sample was digested in sub-boiled HNO_3 at 120 ˚C for 24 hours. All samples analysed for $^{87}Sr/^{86}Sr$ were purified through Sr separation columns using Sr-Spec resin (Horwitz et al., 1992). Dissolved samples were centrifuged for 30 minutes at 5000rpm and loaded on columns equilibrated to 1 mol/L HNO_3. Following this, 0.05 mol/L HNO_3 eluants were used to collect Sr.

2.3 Quadrupole ICP-MS determination of trace elements

Trace element abundances were measured via quadrupole ICP-MS (Q-ICP-MS) on a Thermo Fisher Scientific™ iCAP-Q at the Geochemistry Laboratories at Trinity College Dublin. In preparation for analysis, a 0.1 ml aliquot of each of the solutions was sub-sampled and diluted to produce a 2% (v/v) HNO_3 solution bearing a mixed internal standard with ^{6}Li, Rh, Re, Bi and ^{235}U. Experiments were run following the method outlined initially by Eggins et al. (1997), with some adaptations to the method for different sample matrices and instrument configurations as reported elsewhere (e.g. Babechuk et al., 2010 for silicate rocks; Lawrence et al., 2006a, 2006b for natural waters). Processing of instrument response for signal suppression, drift, blank and interference correction, and calibration were performed offline (e.g., Ulrich et al., 2010). Calibration applied preferred concentrations for the United States Geological Survey (USGS) standard W-2a (Babechuk et al., 2010). Experiment specific and long-term compiled trace element abundances determined for several standard reference materials are used to constrain the intermediate method precision at 3% RSD (1s) or better (≤1% for the REE) for the reported analytes and monitor accuracy (e.g. Babechuk and Kamber, 2011; Lawrence et al., 2006a). A notable exception is that in waters bearing a significant abundance of Ba and very little Eu (i.e., a high Ba/Eu ratio), the final determination of Eu may

be hindered from BaO^+ production (Lawrence et al., 2006); in these cases, Eu data are not reported. The procedural blank contribution to measured unknowns (plants, soil leaches and sampled waters) was typically well below 1% of the measured intensity, with the exception of the most trace element-depleted stream water (SR39), where the contribution of blanks reached a maximum of 10-15% for some analytes. The blanks in the NH_4NO_3 and H_2O leach methods were <1% (mostly <0.2%).

It is common practice for REE concentrations in aqueous samples to be normalised to that of a composite of the average upper continental crust, such as the so-called Post-Archean Australian Shale composite (Taylor and McLennan, 1985). Here, an alternative normalisation dataset known as MuQ (Mud from Queensland), a sediment composite produced by Kamber et al. (2005) is employed. From the normalised patterns, well-established REE anomalies (REE_n/REE_n*), i.e., deviations from an otherwise smooth pattern from the geogenic source or otherwise resulting from a weathering or aqueous reaction, are calculated. Here, REE_n* is the expected normalised concentration when interpolated from a neighbouring element, which does not exhibit anomalous behaviour. The specific projections employ the geometric calculations from Lawrence et al. (2006a) for La, Ce, Eu, Gd, and Lu. The magnitude of LREE over HREE depletion, i.e., the slope of the overall normalised REE pattern, is expressed as the Pr_n/Yb_n ratio (Pr/Yb ratio: $(Pr/Yb)_n = (Pr/Yb)_{sample}/(Pr/Yb)_{MuQ}$) with values >1 indicating light enrichment, and values <1 indicating heavy enrichment relative to the normalising values. The Dy_n/Yb_n is used in an analogous manner to define the MREE/HREE slope. The over-abundance of Y relative to HREE is expressed numerically using the deviation of the un-normalised Y/Ho ratio, which can be compared to the value of ~27 (average upper continental crust; Kamber et al., 2005) and chondritic values of ~26 (Pack et al., 2007).

2.4 TIMS

Post-elution Sr concentrations were determined to assess the Sr content prior to loading on the filament. Approximately 200 ng of Sr was loaded onto outgassed Re filaments together with 1 µL of a TaF_5 activator to enhance Sr ionisation (Birck, 1986). Strontium isotope analyses were performed on a Thermo Scientific Triton Thermal Ionisation Mass Spectrometer (TIMS) with a 5-cup Faraday multi-collector at University College Dublin (UCD). The instrument was tuned for maximum signal strength, stability and peak shape. Strontium isotopes were measured in static mode using Faraday cups, which were calibrated immediately before each

batch of analyses. A rotation of the Faraday amplifiers was also done during the analysis to eliminate any bias. The cup configuration was as follows; 84 in L1; 85 in C; 86 in H1; 87 in H2 and 88 in H3. To ensure data precision, accuracy, reproducibility and comparability to other international data sources, blank and standard analyses were analysed with each batch of analyses. Sample $^{87}Sr/^{86}Sr$ values are reported relative to a value of 0.710250 for NBS SRM 978. The long-term mean value of this standard in UCD was 0.710260 ± 9 (2SD), in agreement with the value measured over the course of this study 0.710261 ± 5 (n=5). Instrumental mass fractionation was corrected using an exponential law to a $^{86}Sr/^{88}Sr$ ratio of 0.1194. All sample value errors are reported 2SE for within-run precision.

2.5 MC-ICP-MS

$^{87}Sr/^{86}Sr$ of additional plant samples were measured by Multi-Collector Induced-Coupled-Plasma Mass-Spectrometry (MC-ICP-MS) following the procedure detailed in Snoeck et al. (2015). The isotope ratios of the purified Sr samples were then measured on a Nu Plasma MC-ICP Mass Spectrometer (Nu015 from Nu Instruments, Wrexham, UK) at ULB. During the course of this study, repeated measurements of the NBS SRM 987 standard yielded $^{87}Sr/^{86}Sr$ = 0.710214 ± 40 (2SD for 15 analyses). All sample measurements were normalised using a sample-standard bracketing method with the recommended value of $^{87}Sr/^{86}Sr$ = 0.710248 (Weis et al., 2006).

2.6 Statistical analysis

Plant data were processed using a one-way ANOVA (Welch's ANOVA, IBM SPSS Statistics for Macintosh, Version 23.0, Armonk, NY: IBMCorp.) to test the null hypotheses that $^{87}Sr/^{86}Sr$ of vegetation, soil leachates and streamwater varies based on (1) underlying bedrock geology and (2) surficial geology.

Further evaluation of statistical outliers, distribution of the variables and resultant trimming of data was conducted as per outlined in Kootker et al. (2016). Six different geological formation based groups and seven different Quaternary geology based groups were used, identified by formation number and Quaternary sediment code, respectively (Table. 1). Extreme outliers, values that deviate more than three times the interquartile range (IQR) from the median, were removed from the dataset. Shapiro–Wilk's normality test was conducted to assess the

distribution of $^{87}Sr/^{86}Sr$ in each group. Tukey's schematic boxplot was generated to display the intra- and inter-group variations in $^{87}Sr/^{86}Sr$. Levene's test for equality of variances was used to test the null hypothesis of equal variances between the groups.

2.7 Biological Absorption Coefficient (BAC)

The relationship between REE+Y content of the soil extracts and plants is examined using the biological absorption coefficient (BAC) to quantify the natural process of element transfer and translocation rates. This provides an estimate of their individual availability to the plant. The BAC is defined as follows (Miao et al., 2008):

$$\mathrm{BAC} = \mathrm{Lx} / \mathrm{Nx}$$

where, Lx = REE+Y concentration in the dry plant sample and Nx = REE+Y concentration in soil leachate.

This ratio can also be described as a transfer factor ratio (Brioschi et al., 2013). The results were categorised into 5 groups based on the magnitude of the coefficient: BAC > 1000 – very strongly accumulated; from 100 to 1000 – strongly accumulated; from 10 to 100 – moderate absorption; from 1 to 10 – weak absorption, and from 0.1 to 1 – very weak absorption. This follows the structure outlined by Kabata-Pendias, (2001) and Lima e Cunha et al., (2014) but has been altered by a factor of one hundred due to the fact that soil leachate compositions were used rather than bulk soils.

3 Results

3.1 Sr isotopic and concentration data

$^{87}Sr/^{86}Sr$ and Sr concentration ([Sr]) are presented in Table 1 in stratigraphic sequence, based upon the geological formation above which each sample was located. The range in vegetation $^{87}Sr/^{86}Sr$ for the study area is 0.7080 to 0.7130. At four sites, with differing lithologies: (1) Devonian basalt, (2) Ordovician/Silurian shale, (3) Permian sandstone and (4) Carboniferous limestone, soil and streamwater samples were collected at proximal locations to the vegetation and demonstrated a range of 0.7086 to 0.7133 for soil leachates and 0.7081 to 0.7107 for streamwaters. This comparative approach is used to examine the relationship between the chemical and isotope compositions of plants and the soil/lithology of their growth location. When the two soil leachates (H_2O and NH_4NO_3) are compared, in each case the H_2O leachate has a more radiogenic $^{87}Sr/^{86}Sr$ than the corresponding NH_4NO_3 leachate. The concentration of Sr measured in ashed woody plant material ranged from 13.89-48.15 mg/kg. Streamwaters ranged from 82.08-555.1 µg/L (Table 1). [Sr] of soil leachates is given as the leachable fraction normalised to the amount of dry mass used and ranged from 5.509 to 8180 µg/L.

Age	Lithology	Fm No.	Quaternary Sediment	Sample I.D.	Sample Type	Easting[a]	Northing	[Sr] (µg/kg)[b]	$^{87}Sr/^{86}Sr$ ratio	2SE	Lab
Lower - Middle Ordovician	Rhyolite and rhyolitic tuff	34	TLPSsS - Till (Lower Palaeozoic sandstone and shale)	SR23	Tree	308772	267470	20340	0.709892	0.000005	UCD
Ordovician - Silurian (416–488 Ma)	Moffat shale facies; Shale and greywacke	42	TLPSsS	SR20	Tree	290215	275794	13890	0.711931	0.000006	UCD
			"	I24	Grass	292556	275409		0.710787	0.000008	ULB
			Rck - Bedrock outcrop	SR19	Tree	291514	278768	17030	0.710697	0.000006	UCD
			"	SR29	H_2O Soil	"	"	5.509	0.711837	0.000042	"
			"	SR34	NH_4NO_3 Soil	"	"	205.1	0.711616	0.000037	"
			TLPSsS	SR39	Streamwater	290858	278747	138.2	0.709856	0.000006	"
Silurian (416–444 Ma)	Deep marine turbidite sequence; mudstone, sandstone, greywacke, shale and conglomerate	49	Rck	I19 - 1*	Grass	307529	284836		0.711762	0.000007	ULB
			"	I19 - 2*	"	"	"		0.710486	0.000008	"
			Ws - windblown sands	I20 - 1*	"	315817	281292		0.709397	0.000007	"
			"	I20 - 2*	"	"	"		0.709177	0.000010	"
			"	I20 - 3*	"	"	"		0.709179	0.000009	"
			GLPSsS -Gravel (Lower Palaeozoic sandstone and shale)	I27 - 1*	"	262733	283186		0.710315	0.000007	"
			"	I27 - 2*	"	"	"		0.708119	0.000008	"
			"	I27 - 3*	Shrub	"	"		0.708328	0.000012	"
			Rck	I35 - 1	"	311401	263848		0.709302	0.000014	"
			"	I35 - 2	Tree	"	"		0.709377	0.000009	"
			TLPSsS	I91 - 1*	Grass	312843	283959		0.711300	0.000009	"
			"	I91 - 2*	"	"	"		0.711027	0.000008	"
			"	I91 - 3*	Shrub	"	"		0.711445	0.000011	"

Age	Lithology	Fm No.	Quaternary Sediment	Sample I.D.	Sample Type	Easting[a]	Northing	[Sr] (µg/kg)[b]	$^{87}Sr/^{86}Sr$ ratio	2SE	Lab
			"	I92 - 1*	Grass	311143	283373		0.714687	0.000011	"
			"	I92 - 2*	"	"	"		0.710293	0.000009	"
			"	SR18	Tree	293090	284654	21910	0.712990	0.000005	UCD
Devonian	Basalt, andesite, basaltic & andesitic tuff	50	Rck	SR21	Tree	293412	273574	24890	0.708415	0.000005	UCD
			"	SR30	H_2O Soil	"	"	5.632	0.713345	0.000044	"
			"	SR35	NH_4NO_3 Soil	"	"	588.3	0.709520	0.000009	"
			GLPSsS	SR40	Streamwater	294125	274150	187.5	0.709761	0.000005	"
Carboniferous, Mississippian	Marine shelf & ramp facies; Argillaceous dark-grey bioclastic limestone, subsidiary shale	61	TLs - Limestone till	SB8	Tree	288768	287451		0.709867	0.000011	ULB
			"	SW7	Streamwater	"	"		0.708336	0.000007	"
Carboniferous, Mississippian	Waulsortian mudbank; Pale-grey massive limestone	62	TLs	SB11	Tree	274108	244665		0.708417	0.000008	ULB
			"	SW6	Streamwater	"	"		0.708119	0.000007	"
Carboniferous Mississippian (299–359 Ma)	Marine shelf facies; Limestone & calcareous shale	64	Ws	I21 - 1	Shrub	314747	277580		0.709235	0.000015	ULB
			"	I21 - 2	Tree	"	"		0.709566	0.000008	"
			A - Alluvium	I22 - 1	Shrub	303860	276113		0.709521	0.000014	"
			"	I22 - 2	Tree	"	"		0.709682	0.000005	"
			GLs	Bettystown**	H_2O Soil	315076	271501		0.709004	0.000027	-
			GLs	Bettystown**	Vegetation	"	"		0.709010	0.000087	-
			TLs	SB4	Tree	301279	265682		0.708438	0.000012	ULB
			"	SW5	Streamwater	"	"		0.708910	0.000009	"
Carboniferous Mississippian	Marine basinal facies; Dark-grey argillaceous	65	TLs	I26 - 1*	Shrub	287445	288471		0.709575	0.000009	ULB
			"	I26 - 2*	Tree	"	"		0.709248	0.000006	"

Age	Lithology	Fm No.	Quaternary Sediment	Sample I.D.	Sample Type	Easting[a]	Northing	[Sr] (µg/kg)[b]	$^{87}Sr/^{86}Sr$ ratio	2SE	Lab
(299–359 Ma) Visean	and cherty limestone & shale		Cut - cutover raised peat	I28 - 1*	Grass	244235	281550		0.708228	0.000007	"
			"	I28 - 2*	Shrub	"	"		0.708305	0.000013	"
			TNSSs - Till (Namurian sandstones and shales)	I37	"	309440	255596		0.708884	0.000008	"
			TLs	SR24	Tree	304678	250183	48150	0.708589	0.000006	UCD
			"	SR31	H_2O Soil	"	"	84.33	0.708672	0.000005	"
			"	SR36	NH_4NO_3 Soil	"	"	4360	0.708622	0.000005	"
			"	SR41	Streamwater	304146	252118	555.1	0.708281	0.000005	"
			"	Tara**	H_2O Soil	289926	259048		0.708333	0.000028	-
			"	Tara**	Vegetation	"	"		0.708421	0.000035	-
			Rck	Cadbury Hill**	H_2O Soil	268749	234702		0.707979	0.000028	-
			TLs	SB2	Shrub	296620	259360		0.709317	0.000012	ULB
			"	SB6	"	"	"		0.708365	0.000013	"
			"	SW2	Streamwater	"	"		0.708632	0.000007	"
			"	SB3	Tree	304678	250183		0.708347	0.000013	"
			"	SB5	"	277046	240041		0.708376	0.000013	"
			"	SB10	Shrub	"	"		0.708737	0.000012	"
			"	SW1	Streamwater	"	"		0.708417	0.000006	"
Carboniferous (299–359 Ma) Namurian	Sandstone, shale; Fluvio-deltaic & basinal marine (Turbiditic); Shale, sandstone, siltstone & coal	71	TLs	I96 - 1	Grass	300282	271704		0.708677	0.000010	ULB
			"	I96 - 2	Shrub	"	"		0.708911	0.000014	"
			"	I96 - 3	Tree	"	"		0.708937	0.000007	"
			"	Knowth - K1	Grass	299690	273439		0.710756	0.000014	"
			"	Knowth - K2	Shrub	"	"		0.708692	0.000008	"
			"	Newgrange	Grass	300743	272727		0.709201	0.000008	"
			"	SR22	Tree	298981	263940	28590	0.708125	0.000005	UCD

Age	Lithology	Fm No.	Quaternary Sediment	Sample I.D.	Sample Type	Easting[a]	Northing	[Sr] (µg/kg)[b]	$^{87}Sr/^{86}Sr$ ratio	2SE	Lab
			"	New Grange**	H_2O Soil	300889	273030		0.709435	0.000035	-
			"	New Grange**	Vegetation	"	"		0.709210	0.000062	-
			"	Knowth**	H_2O Soil	299445	273587		0.709700	0.000290	-
			"	Knowth**	Vegetation	"	"		0.709372	0.000027	-
			"	Knowth**	H_2O Soil	299427	273586		0.709535	0.000032	-
			"	Knowth**	Vegetation	"	"		0.709224	0.000054	-
			"	SB7	Tree	284377	247292		0.709222	0.000012	ULB
			"	SB9	Shrub	"	"		0.709227	0.000013	"
			"	SW3	Streamwater	"	"		0.708578	0.000009	"
Permian	Redbed facies, sandstone, conglomerate, magnesian limestone, marl evaporite	73	TLPSsS	SR17	Tree	279654	290855	43210	0.709084	0.000005	UCD
			"	SR28	H_2O Soil	"	"	86.53	0.709073	0.000005	"
			"	SR33	NH_4NO_3 Soil	"	"	8180	0.709016	0.000009	"
			"	SR38	Streamwater	279761	290904	82.08	0.710651	0.000008	"
Triassic (200–251 Ma)	Sandstone and mudstone with evaporite; Continental redbed facies, lagoonal & shallow marine	75	A - Alluvium	I31 - 1*	Grass	279680	296247		0.710008	0.000008	ULB
			"	I31 - 2*	Shrub	"	"		0.708955	0.000008	"

Table 1. $^{87}Sr/^{86}Sr$ and Sr concentrations of plant, soil leachates and streamwaters as per geological formation. * (Snoeck et al., 2016), ** (Cahill Wilson and Standish, 2016).[a] location data easting and northing are in Irish National Grid, [b] concentration determined by Q-ICP-MS.

3.2 Statistical assessment of spatial $^{87}Sr/^{86}Sr$ variation

The $^{87}Sr/^{86}Sr$ values of plants were categorised into groups based on underlying (1) bedrock and (2) Quaternary geology. The variance of each group was assessed by the Shapiro–Wilk's normality test and demonstrates that the data are normally distributed. Tukey's schematic boxplot in Figure 2 displays the intra- and inter-group variations in $^{87}Sr/^{86}Sr$. Based on Levene's test for equality of variances, the null hypothesis of equal variances can be rejected as there are differences between the variances in the groups (Table 3). Despite the fact that most groups show an overlap in the range of $^{87}Sr/^{86}Sr$, the mean values of certain groups are statistically different ($p<0.05$) (Table 3), indicating noteworthy differences in the spatial variation of $^{87}Sr/^{86}Sr$ in Co. Meath. Namely, the bedrock formation 42 (slate) ≠ 65 (argillaceous limestone) and 49 (mudstone) ≠ 65 (argillaceous limestone), 71 (Carboniferous sandstone). Quaternary deposit 'Sandstone and shale till' ≠ 'Cut peat', 'Limestone till', 'Windblown sands' (see Table 3).

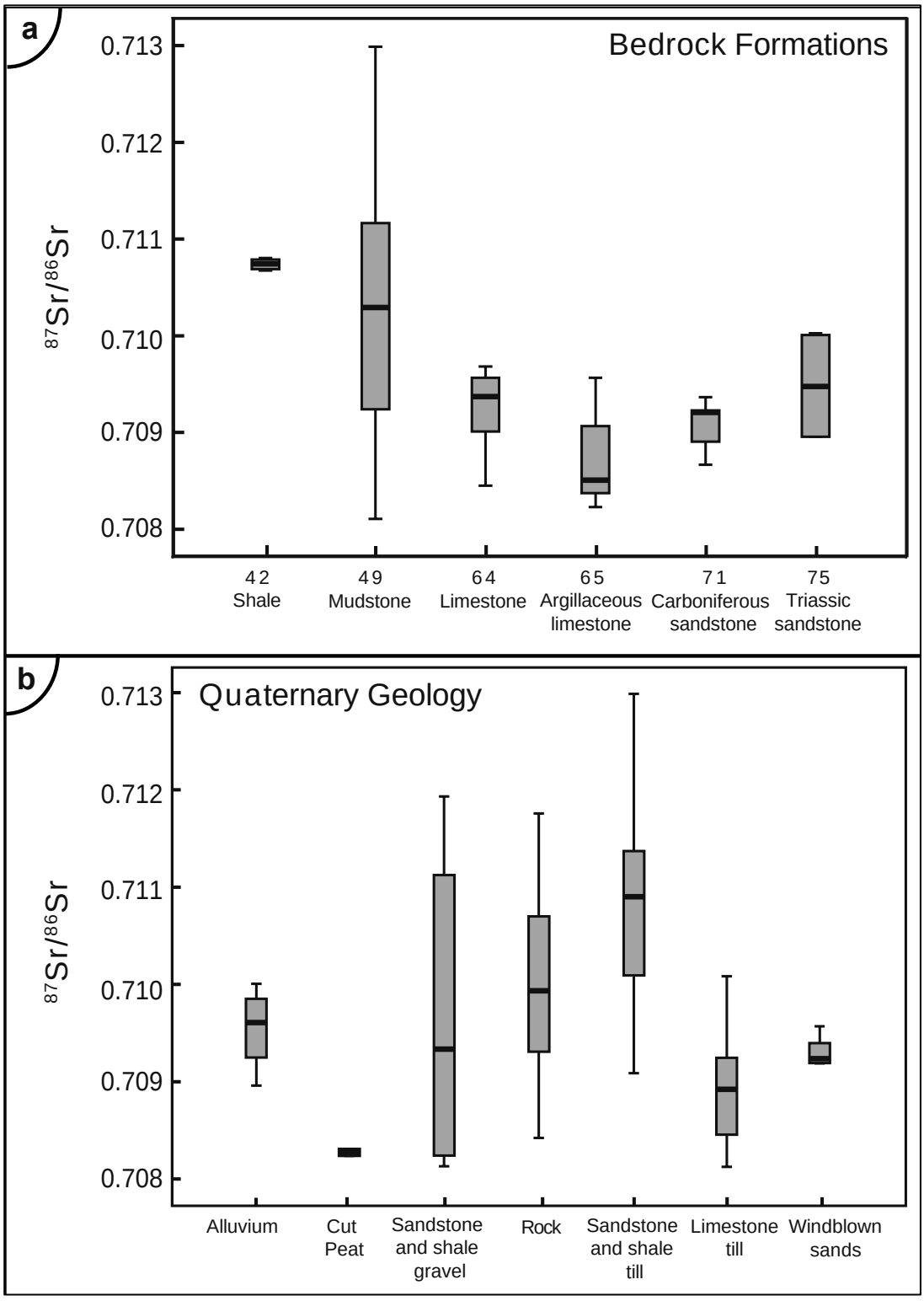

Figure 2. Tukey's schematic boxplot showing $^{87}Sr/^{86}Sr$ variation of each group in Co. Meath. The boxes represent the interquartile range (IQR: Q3–Q1), the central line indicates the median. The whiskers represent Q1−1.5*IQR and Q3+1.5*IQR. For both bedrock and Quaternary geology, there are certain significantly different groups.

Bedrock Formation Statistics	42 - shale	49 - mudstone	49 (w/o outliers)	64 - limestone	65 - argillaceous limestone	71 - Carboniferous sandstone	71 (w/o outliers)	75 - Triassic sandstone
N	2	16	15	6	12	12	10	2
Mean $^{87}Sr/^{86}Sr$	0.710742	0.710449	0.710449	0.709242	0.708699	0.709130	0.709067	0.709482
Standard deviation (1σ)	6.37E-05	1.73E-03	1.36E-03	4.64E-04	4.57E-04	3.85E-07	2.45E-04	7.45E-04
Variance	4.06E-09	3.00E-06	2.00E-06	2.15E-07	2.08E-07	6.20E-04	6.00E-08	5.54E-07
Minimum	0.710697	0.708119	0.708119	0.708438	0.708228	0.708125	0.708677	0.708955
Maximum	0.710787	0.714687	0.71299	0.709682	0.709575	0.710756	0.709372	0.710008
Range	0.000090	0.006568	0.004871	0.001244	0.001347	0.002631	0.000695	0.001053
Median	0.710742	0.710304	0.710293	0.709378	0.708505	0.709205	0.709205	0.709482
Shapiro-Wilk *p* value	-	0.244	0.705	0.340	0.053	0.020	0.058	-

Quaternary Geology Statistics	Alluvium	Cut Peat	Sandstone and shale gravel	Rock	TLPSsS - Sandstone and shale till	TLPSsS (w/o outliers)	TLs - Limestone till	TLs (w/o outliers)	Windblown sands
N	4	2	4	6	9	8	24	23	5
Mean $^{87}Sr/^{86}Sr$	0.709542	0.708266	0.709673	0.710006	0.711278	0.710852	0.708977	0.708900	0.709311
Standard deviation (1σ)	4.40E-04	5.40E-05	1.80E-03	1.20E-03	1.68E-03	1.17E-03	6.08E-04	4.86E-04	1.69E-04
Variance	1.94E-07	2.96E-09	3.00E-06	1.00E-06	3.00E-06	1.00E-06	3.70E-07	2.37E-07	2.84E-08
Minimum	0.708955	0.708228	0.708119	0.708415	0.709084	0.709084	0.708125	0.708125	0.709177
Maximum	0.710008	0.708305	0.711931	0.711762	0.714687	0.71299	0.710756	0.71007	0.709566
Range	0.001053	7.7E-05	0.003812	0.003347	0.005603	0.003906	0.002631	0.001945	0.000389
Median	0.709602	0.708266	0.709321	0.709931	0.711027	0.710907	0.708924	0.708911	0.709235
Shapiro-Wilk *p* value	0.830	-	0.403	0.873	0.468	0.926	0.026	0.185	0.202

Table 2. Descriptive statistics of $^{87}Sr/^{86}Sr$ from plants, for the complete and outlier-trimmed datasets per group.

Bedrock		42 Shale	49 Mudstone	64 Limestone	65 Argillaceous limestone	71 Carboniferous sandstone	75 Triassic sandstone
42	**Mean diff.**	-	0.00058	0.00150	0.00204	0.00161	0.00126
Shale	**Sig.**	-	0.947	0.289	0.002	0.143	0.687
49		-0.00058	-	0.00092	0.00147	0.00110	0.00069
Mudstone		0.95	-	0.248	0.001	0.035	0.895
64		0.00150	0.00092	-	0.00054	0.00018	-0.00024
Limestone		0.289	0.248	-	0.80	1.00	1.00
65 - Argillaceous		0.0020	0.00147	0.0005	-	-0.0004	-0.0008
limestone		0.002	0.001	0.803	-	0.915	0.838
71 - Carboniferous		0.00161	0.00110	0.00018	-0.00037	-	-0.00041
sandstone		0.143	0.035	0.999	0.915	-	0.989
75 - Triassic		0.00126	0.00097	-0.00024	-0.00078	-0.00041	-
sandstone		0.687	0.895	0.999	0.838	0.989	-

Quaternary		Alluvium	Cut Peat	Sandstone and shale gravel	Rock	Sandstone and shale till	Limestone till	Windblown sands
Alluvium	**Mean diff.**	-	0.00128	-0.00013	-0.00047	-0.00131	0.00064	0.00023
	Sig.	-	0.596	1.000	0.978	0.175	0.801	1.000
Cut Peat		0.00128	-	-0.00141	-0.00174	-0.00259	-0.00063	-0.00104
		0.596	-	0.481	0.179	0.006	0.948	0.760
Sandstone and		-0.00013	-0.00141	-	-0.00033	-0.00118	0.00077	0.00036
shale gravel		1.000	0.481	-	0.996	0.281	0.630	0.995
Rock		-0.00047	-0.00174	-0.00033	-	-0.00085	0.00111	0.00070
		0.978	0.179	0.996	-	0.525	0.088	0.822
Sandstone and		-0.00131	-0.00259	-0.00118	-0.00085	-	0.00195	0.00154
shale till		0.175	0.006	0.281	0.525	-	0.000	0.039
Limestone		0.00064	-0.00063	0.00077	0.00111	0.00195	-	0.00041
till		0.801	0.948	0.630	0.088	0.000	-	0.955
Windblown		0.00023	-0.00104	0.00036	0.00070	0.00154	0.00041	-
sands		1.000	0.760	0.995	0.822	0.039	0.955	-

=The mean difference is significant at the 0.05 level

Table 3. Results of the independent sample t-tests comparing mean $^{87}Sr/^{86}Sr$ ratios between the groups. Mean values that are statistically different (p=<.05) are highlighted in grey.

3.3 REE+Y

All pertinent REE+Y ratios are reported along with the abundances in Table 4. The sum REE+Y concentrations vary considerably between sites and between sample media and are given in the order of concentration (see Table 4 for details):

Streamwater: Sandstone >Basalt >Shale >Limestone;
H_2O soil leachate: Basalt >Sandstone >Limestone >Shale;
NH_4NO_3 soil leachate: Basalt >Sandstone >Shale >Limestone;
Plant: Shale>Sandstone>Basalt>Limestone.

Sample Medium	H_2O soil leachate								NH_4NO_3 soil leachate							
Sample I.D.	**SR28**		**SR29**		**SR30**		**SR31**		**SR33**		**SR34**		**SR35**		**SR36**	
Comparative Site	Sandstone		Shale		Basalt		Limestone		Sandstone		Shale		Basalt		Limestone	
		BAC		BAC		BAC		BAC		BAC		BAC		BAC		BAC
(µg/kg)																
Li	2.974	26.9	6.108	60.4	7.201	14.9	1.782	247	13.84	5.77	29.71	12.4	21.70	4.94	3.133	140
Sr	86.53	499	5.509	3090	5.632	4420	84.33	571	8180	5.28	205.1	83.0	588.3	42.3	4360	11.0
Rb	2.376	523	3.751	219	7.685	317	4.392	221	33.05	37.6	94.04	8.74	116.1	21.0	50.06	19.4
Mo	2.115	3.01	0.241	21.5	0.489	562	3.866	8.89	BDL	-	BDL	-	BDL	-	BDL	-
Ba	128.6	857	24.40	5370	73.94	202	118.7	140	20990	5.25	5426	24.2	10520	1.42	16400	1.01
U	3.872	0.32	0.446	7.18	0.695	3.85	1.212	0.99	3.187	0.39	0.435	7.36	0.445	6.00	1.185	1.01
La	5.960	6.48	2.400	37.0	9.178	7.17	6.989	3.70	48.14	0.80	31.55	2.82	308.0	0.21	6.209	4.16
Ce	9.858	5.44	7.906	15.1	42.72	1.75	14.18	2.23	50.35	1.07	59.00	2.02	454.2	0.17	8.158	3.87
Pr	2.205	2.23	0.878	16.6	3.922	2.96	2.139	1.88	9.251	0.53	4.842	3.01	52.65	0.22	1.120	3.58
Nd	10.60	1.77	3.981	13.7	16.58	2.55	9.352	1.57	40.66	0.46	18.80	2.91	188.1	0.23	4.656	3.16
Sm	3.025	1.45	1.042	11.1	3.221	2.28	2.251	1.30	9.834	0.45	3.919	2.96	26.81	0.27	1.032	2.84
Eu	0.842	-	0.268	-	0.760	-	0.542	-	2.616	-	0.960	-	6.025	-	0.176	-
Gd	3.739	1.61	1.119	9.26	2.365	2.74	2.441	1.18	13.57	0.44	4.731	2.19	21.44	0.30	1.028	2.79
Tb	0.563	1.59	0.165	9.11	0.307	2.72	0.372	1.10	1.901	0.47	0.689	2.18	2.569	0.33	0.138	2.96
Dy	3.322	1.53	0.906	8.99	1.590	2.80	2.211	1.01	10.90	0.47	3.772	2.16	12.42	0.36	0.786	2.84
Y	21.22	9.17	4.061	26.0	7.162	12.1	14.80	4.21	109.4	1.78	28.84	3.67	98.71	0.88	6.846	9.10
Ho	0.711	1.51	0.172	9.42	0.297	3.00	0.466	1.00	2.354	0.46	0.731	2.22	2.277	0.39	0.170	2.74
Er	2.036	1.28	0.442	9.42	0.769	2.92	1.267	0.96	6.324	0.41	1.763	2.36	5.306	0.42	0.459	2.64
Tm	0.307	1.05	0.061	9.23	0.107	2.88	0.181	0.93	0.861	0.38	0.218	2.58	0.644	0.48	0.063	2.68
Yb	2.105	0.84	0.362	9.03	0.643	2.76	1.104	0.90	5.263	0.34	1.145	2.86	3.216	0.55	0.380	2.63
Lu	0.347	0.79	0.049	9.90	0.090	3.01	0.162	0.94	0.847	0.33	0.152	3.19	0.426	0.64	0.059	2.59
ΣREE+Y	66.83		23.81		89.71		58.46		264.1		129.6		874.9		25.07	
Ratios:																
Rb/Sr	0.03		0.68		1.36		0.05		0.00		0.41		0.16		0.01	
Ba/Sr	5.92		19.1		56.0		5.98		1.51		23.5		14.9		3.15	
Y/Ho	29.8		23.6		24.2		31.8		46.5		39.4		43.4		40.3	
La/La_n*	1.08		0.97		0.72		1.07		1.73		1.69		1.28		1.65	
Ce/Ce_n*	0.66		1.25		1.41		0.89		0.73		1.45		0.94		0.93	
Eu/Eu_n*	1.04		1.01		1.07		0.98		1.08		1.08		1.19		0.73	
Gd/Gd_n*	1.13		1.09		1.05		1.07		1.23		1.14		1.14		1.13	
Lu/Lu_n*	1.02		0.97		0.98		1.01		1.11		1.07		1.12		1.10	
Dy_n/Yb_n	0.87		1.38		1.36		1.11		1.14		1.82		2.13		1.14	
Pr_n/Yb_n	0.40		0.93		2.34		0.74		0.68		1.63		6.29		1.13	

Table 4. Key trace element concentrations with instructive ratios, and Biological Absorption Coefficients (BAC). BDL: below detection limit.

Sample Medium	Vegetation								Streamwater			
Sample I.D.	**SR17**	**SR18**	**SR19**	**SR20**	**SR21**	**SR22**	**SR23**	**SR24**	**SR38**	**SR39**	**SR40**	**SR41**
Comparative Site	Sandstone	Mudstone	Shale	Shale	Basalt	Sandstone	Rhyolite	Limestone	Sandstone	Shale	Basalt	Limestone
(µg/kg)									**(µg/L)**			
Li	79.85	135.6	368.8	176.6	107.1	50.91	143.9	439.7	0.302	0.659	1.894	1.867
Sr	43210	21910	17030	13890	24890	28590	20340	48150	82.08	138.2	187.5	555.1
Rb	1242	1484	822.0	1032	2438	459.2	1276	970.6	0.673	0.220	0.984	1.037
Mo	6.369	6.965	5.188	3.605	274.8	21.39	3.763	34.38	0.527	0.040	0.217	2.544
Ba	110200	33200	131100	154000	14960	12290	102600	16560	65.79	65.35	114.5	69.96
U	1.251	0.400	3.200	2.024	2.672	1.153	1.088	1.195	0.122	0.159	0.507	1.827
									(ng/L)			
La	38.61	30.76	88.87	100.8	65.84	13.84	51.72	25.85	158.1	14.29	12.72	8.793
Ce	53.64	28.05	119.0	131.7	74.93	24.13	66.48	31.55	128.2	6.899	17.73	11.22
Pr	4.923	4.762	14.58	17.83	11.59	2.956	8.253	4.010	52.35	3.992	3.288	2.312
Nd	18.71	17.52	54.65	65.83	42.34	11.72	31.38	14.71	258.1	18.99	15.46	10.78
Sm	4.376	3.861	11.60	14.81	7.332	2.367	6.579	2.928	64.94	4.543	4.320	3.244
Eu	-	-	-	-	-	-	-	-	15.72	BDL	BDL	BDL
Gd	6.030	4.691	10.36	15.72	6.481	2.266	6.621	2.870	75.13	5.631	4.510	3.540
Tb	0.896	0.655	1.503	2.249	0.835	0.320	0.921	0.408	9.783	0.796	0.658	0.499
Dy	5.068	3.187	8.142	11.19	4.453	1.882	4.956	2.233	56.21	4.992	4.449	3.898
Y	194.6	75.93	105.7	223.3	86.34	210.5	81.42	62.32	414.1	43.54	45.29	44.00
Ho	1.075	0.566	1.620	2.048	0.892	0.453	0.986	0.465	12.39	1.094	1.101	0.979
Er	2.614	1.169	4.163	4.813	2.245	1.184	2.418	1.211	36.82	3.299	3.271	3.117
Tm	0.323	0.132	0.563	0.616	0.308	0.183	0.307	0.169	5.640	0.500	0.519	0.534
Yb	1.776	0.671	3.269	3.531	1.772	1.207	1.708	0.998	39.92	3.205	3.514	3.728
Lu	0.275	0.098	0.485	0.540	0.271	0.210	0.252	0.153	7.501	0.547	0.559	0.691
ΣREE+Y	332.1	172.4	424.6	595.7	307.1	273.6	264.1	150.3	1335	105.7	117.4	97.34
Ratios:												
Rb/Sr	0.01	0.03	0.02	0.04	0.05	0.01	0.02	0.02	0.06	0.01	0.04	0.01
Ba/Sr	0.87	0.64	2.40	5.19	0.31	0.18	1.75	0.30	6.01	3.54	4.58	0.95
Y/Ho	181	134	65.3	109	96.8	465	82.6	134	33.4	39.8	41.1	45.0
La/La_n*	1.95	1.50	1.47	1.33	1.30	1.27	1.56	1.49	1.26	1.39	1.47	1.42
Ce/Ce_n*	1.27	0.66	0.94	0.83	0.72	0.99	0.94	0.88	0.37	0.25	0.78	0.69
Eu/Eu_n*	-	-	-	-	-	-	-	-	0.97	-	-	-
Gd/Gd_n*	1.18	1.18	1.04	1.11	1.12	1.08	1.11	1.08	1.21	1.18	1.09	1.13
Lu/Lu_n*	1.19	1.22	1.08	1.13	1.12	1.12	1.12	1.10	1.12	1.13	0.99	1.12
Dy_n/Yb_n	1.58	2.62	1.37	1.75	1.39	0.86	1.60	1.24	0.78	0.86	0.70	0.58
Pr_n/Yb_n	1.07	2.73	1.71	1.94	2.51	0.94	1.86	1.54	0.50	0.48	0.36	0.24

Table 4. Continued.

3.3.1 Soil leachates

The H_2O leachate of the soils exhibit variable total REE+Y concentrations (23.81-89.71 µg/kg), as well as distinct REE+Y patterns and anomalies (Fig. 5). Y/Ho of the soil associated with shale and basalt are lower at 23.59-24.15 compared to the sandstone and limestone with higher values of 29.84-31.76. The latter trend is mirrored by a negative Ce anomaly in the shale and basalt soil (0.66-0.89 and a positive Ce anomaly in the sandstone and limestone soils (1.25-1.41). The La, Eu, and Lu anomalies are near unity (i.e., within the boundaries of 0.95-1.05 typically indicating a lack of resolvable anomaly) for most samples, apart from a slight positive Eu anomaly (1.07) and negative La anomaly (0.72) in the basalt soil. A minor Gd anomaly is present in all soils (1.05-1.13). The slope of the REE patterns are variable with Dy_n/Yb_n ranging from 0.87 to 1.38, increasing in the order of shale>basalt>limestone>sandstone soils and Pr_n/Yb_n ranging from 0.40 to 2.34, increasing in the order of basalt>shale>limestone>sandstone.

The NH_4NO_3 leachate of the soils also exhibit highly variable total REE+Y concentrations (25.07-874.9 µg/kg) (Fig. 5). Y/Ho of the soils range from 39.42-46.46 and those associated with shale and basalt are lower at 23.59-24.15 compared to the sandstone and limestone (29.84-31.76). The Ce anomalies in the basalt and limestone soils are minor (0.93 and 0.94 respectively), negative in the sandstone (0.73), and positive in the shale (1.45). The Eu anomalies range from 0.73-1.19, with the highest recorded in the basalt soil. All soils record positive La, Gd, and Lu anomalies, ranging from 1.28-1.73, 1.13-1.23, and 1.07-1.12, respectively. The MREE/HREE slope is only slightly positive in the limestone and sandstone with Dy_n/Yb_n both around 1.14, but higher in the shale (1.82) and basalt (2.13). The overall LREE/HREE slope ranges from 0.68 to 6.29, increasing in the order of basalt>shale>limestone>sandstone. Relative to the H_2O leaches (Figure 5c), the NH_4NO_3 leachates release more of the exchangeable/bioavailable REE+Y, as indicated by the higher REE+Y concentrations, with the exception of the limestone soil leachate (lower in NH_4NO_3 leached sample). Moreover, the NH_4NO_3 leachates from the same soils exhibit greater LREE/HREE enrichment with patterns increasing gradually from Lu to La and higher anomalies (preferential leaching) of the La, Ce, Gd, Y, and Lu.

3.3.2 Vegetation

The total REE+Y concentrations of selected vegetation samples (SR17-SR24) ranged from 150.3 to 595.7 µg/kg, with a mean of 315.0 µg/kg ± 142.9 1 SD (n=8). The MREE/HREE slopes are generally consistent with Dy_n/Yb_n a mean of 1.55 ± 0.51 (n=8), with the exceptions of one mudstone/shale sample (SR18 = 2.62) and one sandstone sample (SR22 = 0.86). The overall REE+Y pattern slopes are flat to LREE/HREE enriched with Pr_n/Yb_n ranging from 0.94 to 2.73 with a mean Pr_n/Yb_n ratio of 1.79 ± 0.63 (n=8). All vegetation samples exhibit positive La, Gd, and Lu anomalies (>1.05) and negative Ce (mean of 0.90 ± 0.18, n=8). The most striking feature of the vegetation samples is the strong enrichment in Y relative to Ho, with Y/Ho ranging from 65.28-465.1 (Table 4).

The REE+Y and [Sr] can be separated quite readily based on the BAC classification scheme as the latter is strongly to very strongly concentrated in most the studied plants relative to the H_2O soil leachates and weakly to moderately concentrated relative to the NH_4NO_3 soil leachates (Sr BAC ranges from 499-4420 for H_2O leach and from 5.28-83.0 for NH_4NO_3 leach). Relatively high BAC of Y is evident for both H_2O (range: 4.21-26.0) and NH_4NO_3 soil leachates (range: 0.88-9.10).

3.3.3 Dissolved load in streamwater

The total dissolved REE+Y concentrations (ΣREE+Y) of streamwaters are low and variable, ranging from 97.34 to 1335 ng/L. The highest concentrations are observed in streamwater that drains terrain overlying Permian sandstone (sample SR38) whilst the sample with the lowest sum REE+Y concentration drains carbonate terrain (sample SR41). This is the inverse of [Sr] for the same samples. All streamwater samples are notably depleted in LREE relative to HREE, with a $(Pr/Yb)_n$, range from 0.24 to 0.50 (Table 4; Figure 7). Moreover, all streamwater samples are characterised by negative Ce anomalies (0.25-0.78, n = 4) and superchondritic Y/Ho ratios ranging from 33.43 to 44.96 (mean 39.83 ± 4.80; n = 4). The majority of streamwaters exhibit positive La (1.26-1.47), Gd (1.09-1.21), and subtly positive Lu (0.99-1.13) anomalies. The Eu abundance was only detectable in the most REE+Y enriched streamwater sample (SR38) and does not exhibit an Eu anomaly ($Eu/Eu_n^* = 0.97$).

4 Discussion

4.1 Sr isotope and concentration data

The range in $^{87}Sr/^{86}Sr$ of modern plants over the study area is 0.7080 to 0.7130. There is a lack of agreement between the $^{87}Sr/^{86}Sr$ measured in different sample media overlying basalt, shale and sandstone (Figure 3). However, vegetation, soil leachates and streamwater associated with limestone bedrock (Formations 64 and 65) have a much smaller range in $^{87}Sr/^{86}Sr$ (0.7082-0.7097), fitting closely with the relatively narrow range of previously measured biosphere samples in Carboniferous limestone regions of Britain: 0.7089 (soil leach n=5), 0.7092 (plant n=11), 0.7099 (water n=7) (Evans et al., 2010). The Waulsortian (upper Tournaisian – lower Visean) limestone underlying much of Co. Meath has an average $^{87}Sr/^{86}Sr$ of 0.7079 (±0.0009, n=23)(Douthit et al., 1993). This value reflects Visean seawater composition which is inferred from the analysis of well-preserved marine fossils (0.7075-0.7082) (Burke et al., 1982; McArthur et al., 2001). Similarly, Visean limestones on the Isle of Man yielded $^{87}Sr/^{86}Sr$ of 0.7079 (n=2) (Hendry et al., 2015). The mean of all limestone-associated biosphere values in this study, 0.7089 ± 0.011 (n=11), is higher than these published whole rock values, indicating an additional more radiogenic source. This can result from the leaching of more silicate-rich fractions in the surficial sediments or the input of contemporary rainfall with values generally close to that of seawater but which can be higher (ca. 0.7095) depending on dust contribution (Bain and Bacon, 1994; Négrel et al., 2007). Moreover, the naturally leachable fraction of bedrock likely does not equate to that of the bulk rock $^{87}Sr/^{86}Sr$. The water-soluble Sr of carbonates were found to vary from 0.23% to 1.3% of the total rock composition (Bailey et al., 2000). Both the water soluble and 1 mol/L ammonium acetate leached fractions produced higher $^{87}Sr/^{86}Sr$ than the bulk rock due to the dissolution of groundwater salts, contaminant Sr on ion-exchange sites and a weak dissolution of calcite (Bailey et al., 2000).

Devonian basalt provides the highest range of $^{87}Sr/^{86}Sr$ values across all sample media, 0.7084 (vegetation) - 0.7133 (H_2O soil leachate) (Fig. 3). The large range is somewhat misleading as the H_2O leach provides an exceptionally high $^{87}Sr/^{86}Sr$ value that is a statistical outlier. Biosphere values above basalt formations within Britain and Ireland

generally do not demonstrate comparably radiogenic values. The range of previously measured biosphere samples (soil, plant, water) overlying basalt in the UK is 0.7061 – 0.7105 (Evans et al., 2010) and in Northern Ireland, which hosts expansive basalts, overlying modern plant samples have been found to have an average value of 0.7089 ± 0.0037 2SD (Snoeck et al 2016). The vegetation and streamwater $^{87}Sr/^{86}Sr$ from the basalt in this study region have much less radiogenic values; 0.7084 and 0.7098 respectively, which are more likely representative of the local biosphere values.

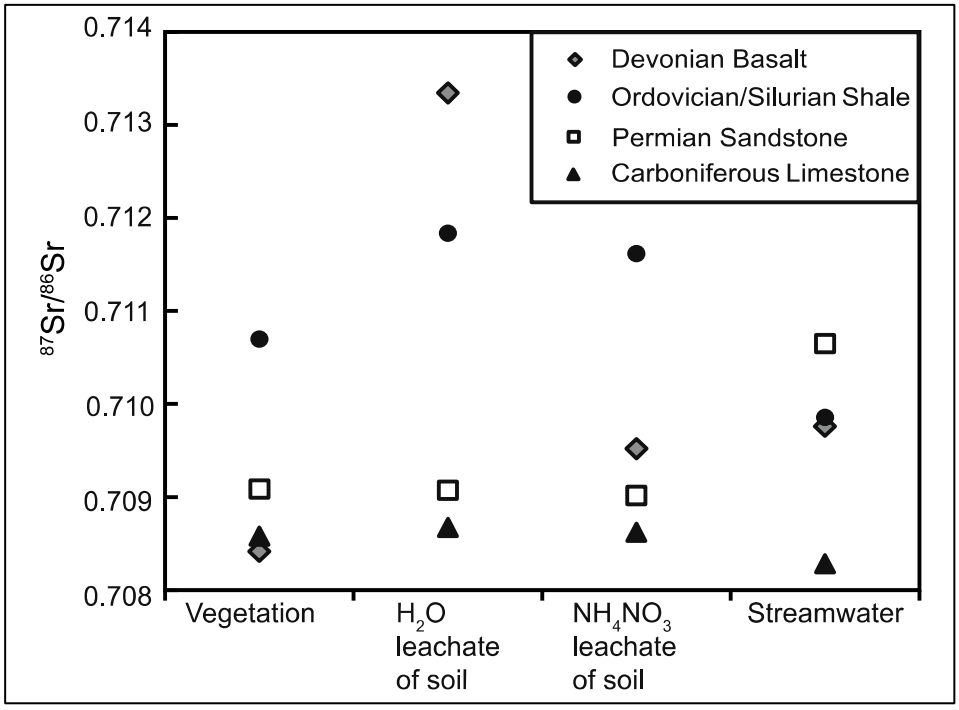

Figure 3. $^{87}Sr/^{86}Sr$ for sample media at four comparative sites in Co. Meath with differing underlying geology. Whilst the $^{87}Sr/^{86}Sr$ of each sample medium overlying the limestone bedrock is relatively invariable, the $^{87}Sr/^{86}Sr$ of different samples at the other three sites show more variation, highlighting a higher degree of complexity in Sr transfer.

Streamwater [Sr] in the region displays a wide spread of values (ranged between 82.08-555.1 µg/L), highlighting the complex nature of Sr in the hydrological system of Co. Meath. These concentration data correspond with probable values for the underlying lithology, with concentrations increasing from sandstone < shale < basalt < limestone bedrock. The Quaternary deposit types also correspond with measured streamwater [Sr], showing that streams draining limestone rich tills are the most concentrated in Sr and have the least radiogenic isotope values. Conversely, those draining Lower Palaeozoic sandstone tills have lower concentrations and more radiogenic $^{87}Sr/^{86}Sr$.

The streamwater draining an area with only very thin Lower Palaeozoic sandstone till coverage with outcrops of Permian sandstone bedrock has the lowest concentrations and the highest $^{87}Sr/^{86}Sr$ of the sampled streamwaters. Therefore, both the $^{87}Sr/^{86}Sr$ and [Sr] reflect mixing of bedrock and surficial sediments.

4.2 Suitability of sample media used for bioavailable Sr mapping

Establishing geochemical relationships between soil/plants and streamwater geochemistry makes it possible to determine which sample media are most informative for geographical discrimination studies. Both soil and plants have been employed in previous studies for producing biosphere isoscapes (Evans et al., 2010; Frei and Frei, 2013; Hartman and Richards, 2014; Hodell et al., 2004; Laffoon et al., 2012; Nafplioti, 2011; Porder et al., 2003; Price et al., 2014; Price and Naumann, 2015; Sjögren et al., 2009; Willmes et al., 2014) but it is not agreed which sample medium is most appropriate for this purpose. Most of the debate centers on soils and their disposition for variability. Owing to the fact that the mineral components of soils are inherited from geological parent materials that have been weathered to varying degrees, the bioavailable soil solution is not always in equilibrium with the soil-mineral component (Kabata-Pendias, 2001).

The $^{87}Sr/^{86}Sr$ of natural mineral waters have demonstrated a good correlation with estimated values based on the local geology (Montgomery et al., 2006b; Voerkelius et al., 2010). Correspondence between plant $^{87}Sr/^{86}Sr$ and other media such as snails and small home-range fauna have also been noted (Blum et al., 2000; Laffoon et al., 2012). The NH_4NO_3 soil leachates and plants collected across France (Willmes et al., 2014) are correlated ($R^2 = 0.89$). Warham (2011) also made comparisons between vegetation, H_2O soil leachates and streamwater from different geological settings. Again, there is a strong correlation between the mean values of each sample type in their geological group (n = 30 plant, 30 streamwater, 26 soil leaches), but within each of the chronostratigraphic groups, the standard deviation of the soil data is almost an order of magnitude greater than the associated plant and streamwater values, with the soil leaches giving consistently more radiogenic values than both plants and waters.

Here, when two soil leachates (H_2O and NH_4NO_3) of the same soil are compared, in each case the H_2O leach has more radiogenic $^{87}Sr/^{86}Sr$ than its NH_4NO_3 counterpart (Fig. 3). This finding suggests the latter leaches more Sr from less radiogenic carbonate minerals due to the increased aggressiveness of the NH_4NO_3 towards such mineral weathering products (cf. Frei and Frei, 2013; Warham 2011). The deionised H_2O leach was potentially not aggressive enough to replicate natural dissolution of primary and secondary carbonate minerals and therefore does not achieve values similar to those seen in plant and streamwater and does not represent the bioavailable fraction of the soil. Overall, the $^{87}Sr/^{86}Sr$ range in soil leachates is determined by the specific leaching method chosen and therefore, careful selection of an appropriate leaching protocol, in this case NH_4NO_3, is necessary for informative estimates of the natural ranges that exist within the pedosphere. Based on results from this study, soil leachates provide a larger range of $^{87}Sr/^{86}Sr$ than vegetation and are thus less effective at estimating local bioavailable $^{87}Sr/^{86}Sr$ ranges. This is in agreement with others studies (Evans et al., 2010; Evans and Tatham, 2004; Maurer et al., 2012; Poszwa et al., 2002; Montgomery et al., 2003) that also conclude soil leachates are a poor material for mapping local $^{87}Sr/^{86}Sr$ as they can produce more variable $^{87}Sr/^{86}Sr$, that are inconsistent with the associated plant data. Thus, plant material provides a more direct estimate of bio-available $^{87}Sr/^{86}Sr$ and can average out short-term or seasonal variations in the soil composition.

4.3 Relationship between bedrock/Quaternary geology and biosphere

Thick glacial deposits (>10 m depth in most areas) of differing composition are extensive across Co. Meath. Consequently, there is strong potential for these surficial glacial deposits to contribute to the Sr biosphere budget. Both the underlying bedrock (Figure 4 a) and Quaternary surficial geology (Figure 4 b) are examined as controlling factors of biosphere $^{87}Sr/^{86}Sr$.

Based on discriminant analysis, using $^{87}Sr/^{86}Sr$ as descriptors, there were significant differences ($p>0.05$) in the mean $^{87}Sr/^{86}Sr$ of plants between both the different bedrock formations (n=47, categorised into 6 groups) and Quaternary geology (n=52, categorised into 7 groups). Notably, formation 49, Silurian mudstone was significantly different statistically ($p<0.05$) from both Formations 65 (Visean limestone) and 71 (Carboniferous shale/sandstone). In addition, the mean difference of biosphere samples

overlying the two primary Quaternary geology groups (limestone till (n=24) and Lower Palaeozoic sandstone and shale till (n=8)) was statistically significant (Table 3). The $^{87}Sr/^{86}Sr$ signature of these samples therefore reflects both the underlying geology and, to a significant degree, the superficial Quaternary geology. The surficial deposits in this region homogenise with the local bedrock signatures and thus, the measured signatures reflect the averaging of these two prominent geochemical reservoirs.

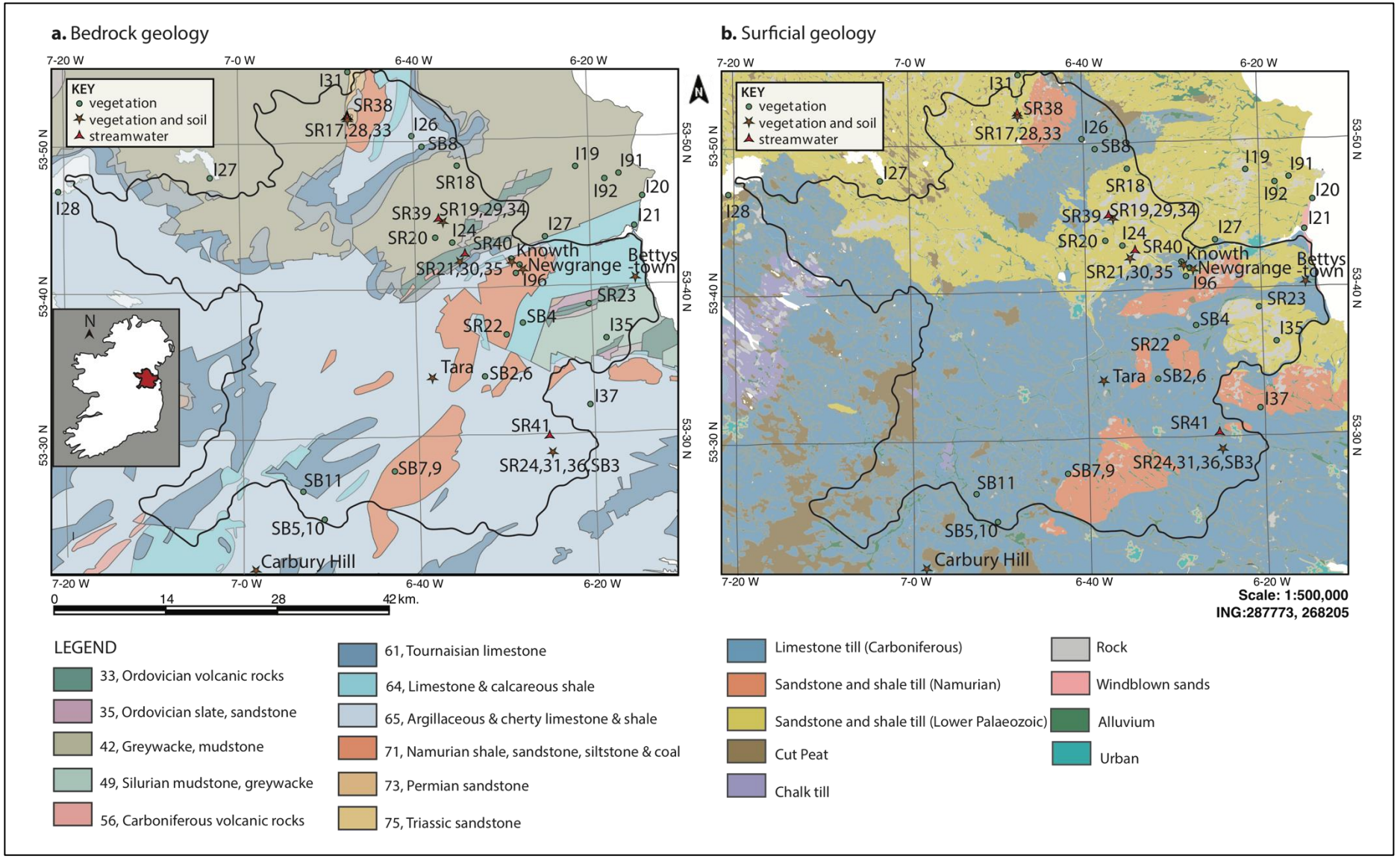

Figure 4. (a) Bedrock and (b) Quaternary geology of Co. Meath with sample sites. Basemap from Geological Survey of Ireland, (2016).

4.4 Archaeological implications

Element cycling from bedrock through to the biosphere underpins isotopic geographical discrimination. Characterising the distribution of Sr in the biosphere of Co. Meath and the surrounding area is of particular interest owing to the region's rich archaeological heritage, with internationally renowned sites such as Newgrange, Tara and Knowth. Based on the statistical and observed results of this study, Co. Meath has distinct $^{87}Sr/^{86}Sr$ packages within the local biosphere that correlate, to varying degrees, with both underlying bedrock and superficial sediments. Therefore, it is possible to use this isotope system as a provenance indicator for archaeological case studies based within this region, with caution not to base interpretations on bedrock geology composition alone.

Whilst the overall $^{87}Sr/^{86}Sr$ range (0.7080 to 0.7130) of plants across the entire studied region is not geographically unique when compared with values already known for Ireland and to the more regionally comprehensive database for Britain, there are nonetheless distinctive divisions of the biosphere. For comparison, plants collected across Britain have a range of 0.7077 (chalk bedrock) to 0.7266 (granite bedrock) (Evans et al., 2010; Montgomery et al., 2006b). The $^{87}Sr/^{86}Sr$ of modern plants from the north of Ireland demonstrate a range of 0.7067 (basalt bedrock) to 0.7195 (granite bedrock), excluding those values deemed as outliers (Snoeck et al. 2016). This highlights that there are regions of Ireland which have measured biosphere $^{87}Sr/^{86}Sr$ lower and higher than the range in Co. Meath (0.7080 to 0.7130), as expected.

Granite and a combination of Lower Palaeozoic and late Pre-Cambrian metamorphic rocks are found in the West of Ireland (Fay et al., 2007). Due to the extensive age of these rocks, they are likely to have higher $^{87}Sr/^{86}Sr$ that other parts of the country. Northern Ireland comprises schists and quartzites and high $^{87}Sr/^{86}Sr$ values are exhibited in granitic gneisses (0.7603-0.7676), shales (0.7196-0.7273) and diorites (0.7126-0.7217) in south east Ireland (Davies et al., 1985). Tertiary basalts in the northeast of Ireland are relatively young and low in Rb and therefore exhibit less radiogenic $^{87}Sr/^{86}Sr$, ~0.703-0.708 (O'Connor, 1988; Wallace et al., 1994) and a porcellanite from the north of Ireland was found to have mean $^{87}Sr/^{86}Sr$ values of 0.7044

(± 0.0004, n=12)(Curran et al., 2001). The $^{87}Sr/^{86}Sr$ of modern plants collected across Northern Ireland ranged between 0.7067 (above basalt bedrock) to 0.7195 (above granite bedrock) (Snoeck et al., 2016).

Although these values are measured from whole rocks, they indicate that the biosphere components can source Sr from rock reservoirs with $^{87}Sr/^{86}Sr$ values both below and above the range exhibited in Co. Meath. This allows archaeological remains of individuals local to this area to be distinguished from those originating from such isotopically distinct regions of Ireland or from further afield. Using $^{87}Sr/^{86}Sr$ for geographic discrimation of regions to trace origin can also be informative when compared with more radiogenic environments such as Scandinavia. The higher $^{87}Sr/^{86}Sr$ values that characterise parts of Northern European regions, and hence the people who inhabited them, allow such individuals to be discerned from those who were local to Co. Meath or the surrounding area (cf. Knudson et al. 2012).

Dentine can exchange varying proportions (15-100%) of biogenic Sr with soil from its burial environment making it unreliable as a reservoir of biogenic Sr (Budd et al., 2000). It is because of this exchangeability of Sr with soil that measured dentine $^{87}Sr/^{86}Sr$ values are sometimes used as a proxy for the local range in biosphere $^{87}Sr/^{86}Sr$ values (Evans et al., 2010; Montgomery et al., 2007). In such cases, dentine $^{87}Sr/^{86}Sr$ values are used in combination with the co-genetic enamel and Sr concentrations to define a diagenetic vector. The inconsistency of soil leachates with vegetation data in this study suggest that using dentine, derived from archaeological dental remains that were buried and equilibrated with surrounding soil, may be erroneous for establishing such a vector towards biologically available Sr (BASr) and determining local ranges. The local leached soil does not directly reflect BASr and by inference, neither would exchanged tooth dentine. Plant material is the most appropriate and informative sample type for estimating BASr in this region but owing to small-scale variations, high-density sampling is required.

4.5 REE+Y in the biosphere

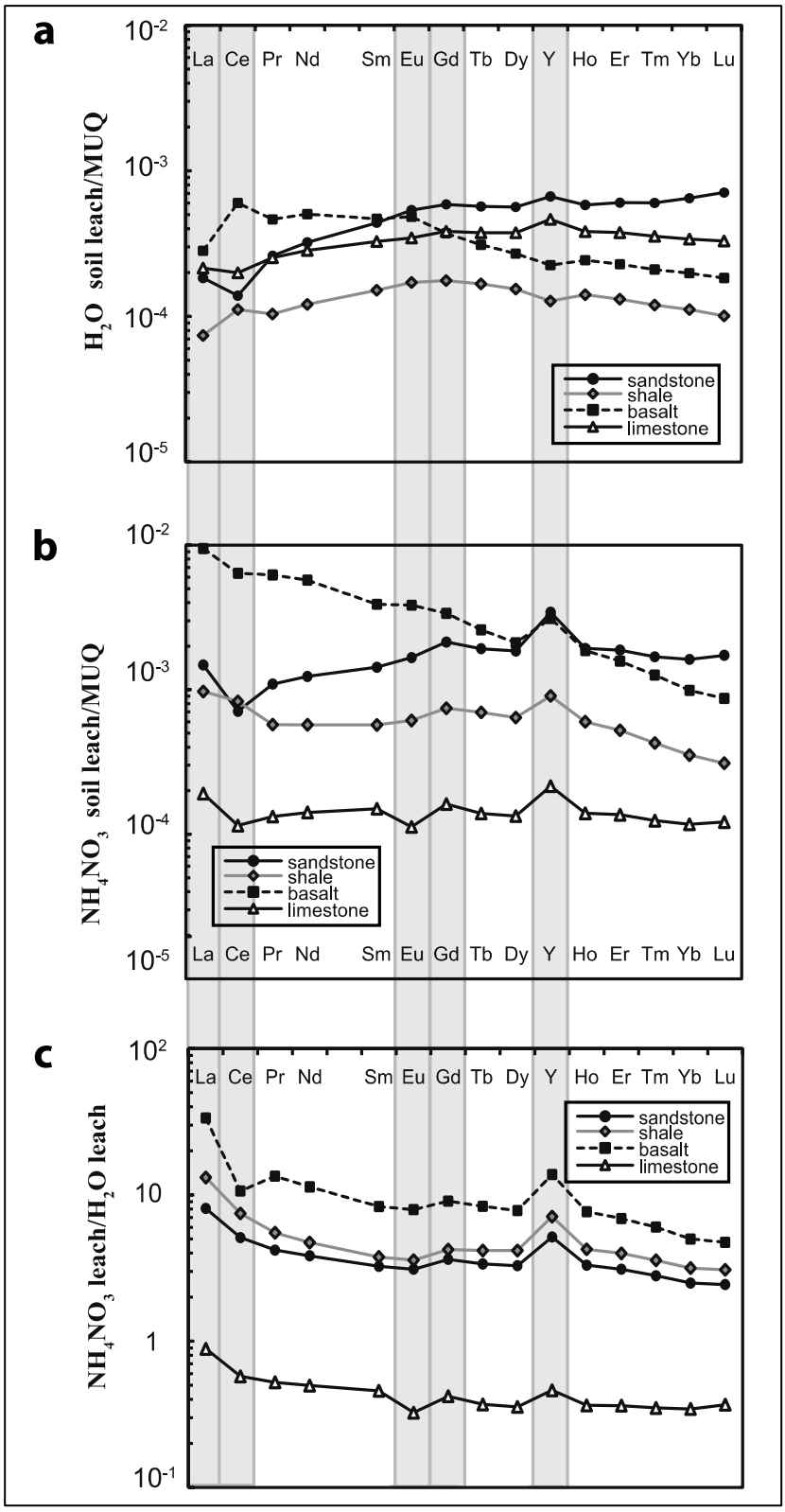

Figure 5. Soil REE+Y of (a) H_2O leachate, (b) NH_4NO_3 leachate and (c) leachates normalised to one another. Key features of REE+Y patterns are highlighted with grey backgrounds. Normalisation value is the modern alluvial sediment composite MUQ (Mud from Queensland) of Kamber et al. (2005).

4.5.1 Translocation of REE+Y from soil to biomass

Just as for the [Sr], there are notable differences between the two leaching methods employed, both in terms of REE concentration and overall pattern (Figure 5). The main comparative bedrock types in this catchment (sandstone, mudstone, basalt and limestone), should have distinct REE and [Sr] based on mineral composition as the distribution of both Sr and REE in various soils typically reflects the geological origin of parent rocks and their mineral composition (Kabata & Pendias 2001). Thus, one might expect the REE pattern and $^{87}Sr/^{86}Sr$ of the soils that have developed on these rocks to reflect, at least to some extent, their geochemical fingerprint. Thus, despite the well-established complexities of REE chemistry in soils (e.g., reflecting a combination of host mineral effects, pH controls, complexation) (Byrne and Sholkovitz, 1996; Deberdt et al., 2002; Elderfield et al., 1990; Lawrence and Kamber, 2006; Matsunaga et al., 2015; Noack et al., 2014; Pédrot et al., 2015a; Tricca et al., 1999) some broad inferences and comparisons can be made from comparing the two soil leaches to each other and to plants associated with soils in terms of their parent rock. When comparing total concentration of REE in soils on the basis of geographical location, those developed on basalt bedrock have relatively higher REE concentrations than the soil developed on sandstone, shale and limestone lithologies. This is broadly consistent with expectations from the different lithologies in terms of their REE contents, with soils originating from igneous rock, sandstone, and shale tending to have higher REE contents than soils developed from loess and calcareous rock (Hu et al., 2006; Loell et al., 2011). In general, the high REE in the basalt-dominated soil indicates the most easily leachable REE fraction, which likely reflects the lack of poorly leachable REE-rich phases and the high abundance of Fe/Mn-oxy(hydroxides) with potentially adsorbed REE. For example, apatite ($Ca_5(PO_4)_3(OH,Cl,F)$) is a conceivable major host of REE in basalt-derived soils and due to apatite weatherability, high abundance of REE, and typical LREE enrichment (Giero and Stille, 2004). These factors could help explain the greatest enrichment of LREE/HREE in the soil leaches from basalt-dominated area through the preferential leaching of REE from its carrier apatite. Also notable is the positive Eu anomaly present only in leaches from the basalt-dominated soil, which likely represents the preferential release of Eu from plagioclase to the soil pore waters (Condie et al., 1995; Huang and Gong, 2001; Ma et al., 2011). Conversely, the lower REE in the sandstone and shale and flatter REE slope to LREE/HREE

depletion reflects the abundance of less leachable REE-host minerals. The NH_4NO_3 leached-soils that developed on the limestone bedrock had the lowest ΣREE. Calcareous soils tend to have relatively low REE contents; carbonate bears relatively low REE concentrations and any non-carbonate phases in limestone (minor amounts of phyllosilicate detritus) would be poorly leachable (Bailey et al., 2000).

For the H_2O leach, the basalt and shale soils show a lower Y/Ho ratio than the normalising composition (i.e., less than ~27), whereas the sandstone and shale show a higher Y/Ho (>27). For all soils, Y shows a preferential release relative to Ho in the NH_4NO_3 leach (higher Y/Ho) (mean Y/Ho = 42.4 ± 3.21 (n=4)) that exceeds that of the H_2O leach (mean Y/Ho = 27.3 ± 4.08 (n=4)). These trends indicate a greater solubility of Y during chemical weathering processes and a greater capacity for Y to be released during leaching and become bioavailable in soils. Previous work has shown that Ho should have a greater retention on Fe/Mn-oxy(hydroxide) surfaces than Y due to their orbital chemistry differences, but organic complexes have a tendency to hinder the competitive adsorption and reduce the overall capacity for Y/Ho fractionation (Babechuk et al., 2015; Thompson et al., 2013).

The presence of positive Ce anomalies in the H_2O leaches of the basalt and shale-derived soils suggest that more easily exchangeable Ce was present and likely reflects a higher abundance of Fe/Mn-oxy(hydroxides). In contrast, a negative anomaly was noted for the NH_4NO_3 leachate of the basalt soil which may reflect dilution by LREE released from other phases. The overall stronger LREE enrichment of NH_4NO_3 over H_2O soil leachates suggests that mineral phases abundant in LREE, are more susceptible to dissolution with the more aggressive leach and thus, NH_4NO_3 preferentially releases LREE adsorbed to soil particulate surfaces. This reflects the overall greater LREE over HREE enrichment in clastic sedimentary rocks and the bulk soils that derive from them (Aide and Aide, 2012; Kabata-Pendias, 2001) It is thus likely that the more aggressive NH_4NO_3 is a more accurate representation of the available REE in these samples.

By comparing REE patterns of soil leachates and trees accessing this nutrient pool, it is possible to address whether the observed REE anomalies in *Fraxinus excelsior L.* are a function of those in soil. The distribution of individual REE in plants showed some

agreement with that in the soil extracts but no clear trends were observed (Figure 6). Generally, the REE released with the H_2O and NH_4NO_3 extraction procedures were poor indicators of REE uptake in plants, with a slightly closer correspondence between the REE of plants with those of the NH_4NO_3 leach, which have relatively flat REE slopes when normalised to one another (mean slope=1.10, n=4). A LREE enrichment (Pr_n/Yb_n) is consistently noted in the plants, to a greater extent than observed for the H_2O leachates (Figure 6b). Notably, the Gd, and Lu anomalies are near uniformity when normalised to the H_2O leachate, indicating that the plants capture these anomalies from the water soluble portion of the soils. Exceptions are the variability in the Ce anomalies (Ce/Ce_n* range from 0.66 - 1.27) that appear to be only represented by the leachates of the limestone. There is a strong over-abundance of Y in all vegetation samples beyond what was released by the NH_4NO_3 or H_2O leached soils. Whilst the water-soluble and exchangeable fraction are operationally defined, they are nonetheless useful for obtaining an estimate of REE bioavailability. As such, it cannot be explicitly deduced that the specific anomalies present in the leached soils are a precursor of those in the terminal branches of *Fraxinus excelsior L*. Nonetheless, the discrepancy between the REE patterns of the sample media indicates that the aerial portion of ash trees do not directly reflect the REE in the bioavailable portion of the soil.

Fractionation of Ce results from changes in oxidation state whilst fractionation of the other REE may be due to differences between plant species or even variations between individual plants of the same species (Wyttenbach et al., 1998). Under oxic conditions Ce(III) is oxidised to Ce(IV) which is less mobile, due to its enhanced adsorption by Fe/Mn oxy(hydroxides), and aids with preferential mobilisation of the trivalent REE (Bau, 1999; Laveuf and Cornu, 2009). Two soil leachate samples (from above shale and basalt) and all plants display a negative Ce anomaly. This is consistent with previous studies demonstrating lesser uptake of Ce(IV) in vascular plants, such as spruce and blackberry (Fu et al., 2001; Wyttenbach et al., 1998). The penetrability of ions through plant membranes decreases with the increase of its valency and therefore even simple ions of Ce(IV) are less penetrable than Ce(III) and thus, dissolved REEs typically exhibit a Ce-depletion (Fu et al., 2001). The negative Ce anomalies in *Fraxinus excelsior L.* support findings that REE behaviour in aerial portions of plants is mainly partitioned in the dissolved phase as it is preferentially scavenged on the roots and is thus less mobile than the other REE, cf. Censi et al. (2014).

The extended trace element suite are peripheral to the main aim of the study, but nonetheless provide an additional distinction between soils and plants associated with different parent materials. For example, the soils developed on shale and basalt have higher alkali element concentrations (Li, Rb) and are readily distinguished from those associated with limestone or sandstone through Rb/Sr ratios (as well as Ba/Sr ratios). In general, similar trends are observed within sample media overlying the varying lithologies. This likely reflects a greater proportion of silicate-associated elements released from the basalt and shale soils relative to the sandstone and limestone soils that are overwhelmed with easily leachable Sr-bearing minerals (e.g., carbonate).

The REE patterns of the trees illustrate an overall similarity to each other, where generally LREE are being fractionated from HREE during migration from the soil and uptake into the plant system and as a result, the BAC is higher for LREE (except for Ce) than HREE. This fractionation was not noted for the bark from *Fraxinus excelsior L.* from environments across France (Agnan et al., 2014). There is a natural tendency for the preferential uptake of available LREE relative to HREE with decreasing transfer of REE with increasing atomic mass. The high abundance of LREE relative to HREE has been widely observed but whether this fractionation occurs during the process of absorption or within the plant tissues themselves is still an ongoing subject of research (references). Rather than the plants indiscriminately absorbing REE, the LREE enrichment of plants may result from plant roots preferentially solubilising LREE in soil surrounding the plant roots over HREE. This LREE enrichment has been taken to reflect the presence of organic acids, ligands, the dissolution of the phosphate phase in the soil and complexation of REE in the rhizosphere (Ding et al., 2006; Fu et al., 1998,2001; Miao et al., 2008; Wang et al., 1997; Wei et al., 2001; Wyttenbach et al., 1998; Zhang et al 2002). Additionally, HREE are preferentially bound to Fe/Mn-oxy(hydroxides) and as a result, LREE are relatively more mobile, and thus are more likely to enrich soil water pool (Brioschi et al., 2013).

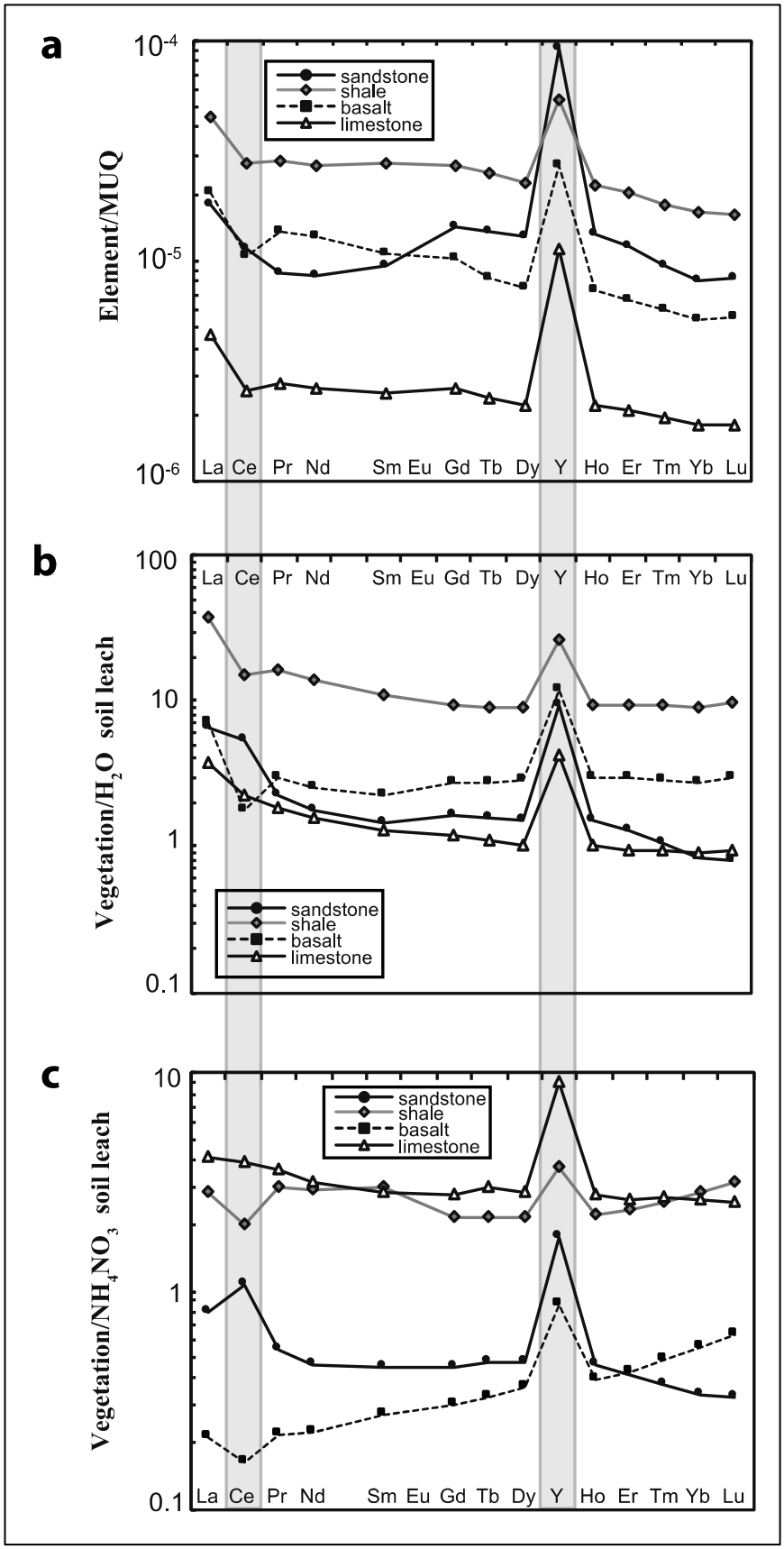

Figure 6. REE+Y of vegetation from comparative sites (n=4) normalised to (a) MUQ, (b) H_2O leachate and (c) NH_4NO_3 leachate.

The REE+Y mostly have very weak to weak absorption coefficients (BAC ranges from 0.84-37.0 for H_2O leach and from 0.17-4.16 for NH_4NO_3 leach), with the exception of Y and La, which are enriched in these plants (Table 4). The high Y/Ho ratio is the most striking characteristic of the REE+Y patterns of tree samples (Figure 6a). Notably, the topsoils are dominantly developed on carbonate-rich tills and the preferential Y enrichment may be consistent with the chemical composition of the local carbonate lithology, which already bears an over-abundance of Y (relative to Ho). However, although the anomaly may in part be attributed to a transfer of the geogenic signature during biouptake, the Y/Ho anomaly in all biomass is much higher than all measured soil leachates and would appear to require a preferential uptake mechanism of Y. At what stage and for what purpose this occurs is speculative (Kastori et al., 2010), but the enhanced aqueous mobility of Y due to its contrasting complexation behaviour in comparison to the lanthanides (Bau et al., 1996) is probably a contributor to the elevated uptake from the soil element budget.

Elevated Y/Ho ratios have also been recorded by Yu et al., (2007) in mangrove tree rings with Y/Ho ratios averaging 124. These values are much higher than expected seawater or shale Y/Ho ratios. Yu et al., (2007) speculated that the relative enrichment of Y to Ho and the other REE is due to the difference in its transportation in the metabolic pathway or its bioavailability in ambient seawater. In another case study, Loell et al., (2011), measured the total REE contents (aqua regia digestion), potentially plant-available (EDTA) and mobile (NH_4NO_3) in loess soils. The authors found that the EDTA fraction represented on average 10.1% of the total REE soil contents with a notably high available proportion of Y (mean 24.8%, max 39%). In addition, Ce was the most abundant REE in the bulk digests but was least abundant in the EDTA fraction emphasising its poor bioavailability. These findings corroborate the REE+Y patterns found in the present study, with depleted Ce and elevated Y concentrations in the plants reflecting their respective lower and higher bioavailability in the potentially-available soil fraction and suggests that elevated Y/Ho in plants may be a common feature.

4.5.2 Dissolved load in streamwater

The MuQ-normalised REE patterns of sampled streams are similar overall, varying mostly in concentrations, and bearing a strong resemblance to the those of seawater or groundwater (Figure 7), of which the characterising features are a steep LREE/HREE depleted pattern, negative Ce anomaly, and over-abundance of La, Gd, and, to a lesser extent, Lu (see Kamber et al., (2014) for a discussion of these features). Aquatic fractionation is unlikely to explain the pervasive streamwater-like features, such as the high Y/Ho ratios in the range of 33-45, consistent negative Ce anomaly, and low Pr_n/Yb_n compared to larger river systems (Elderfield et al., 1990), since Ce and Y are not expected to fractionate significantly in freshwater (Lawrence et al., 2006a, 2006b; Möller et al., 2003). The primary control on the streamwater signatures is interpreted to reflect a predominance of carbonate in the catchments (either bedrock or surficial sediments), such that the streamwaters inherit the palaeo-ocean chemistry from which the carbonate was precipitated. As rainwater percolates through the soil and carbonate-rich sediments and enters the streams by means of run-off, the freshwater flowing off these small catchment systems manages to obtain the seawater-like trace element geochemical fingerprint. This finding is in agreement with the conclusions of several other investigations analysing terrestrial waters, showing that rivers, groundwater and lakes can have HREE enriched patterns that resemble those of modern seawater (e.g. Elderfield et al. 1990; Smedley 1991; Johannesson & Lyons 1994; Sholkovitz 1995; Johannesson et al. 1999; Tricca et al. 1999; Johannesson & Hendry 2000; Johannesson et al. 2006). Nevertheless, the degree of fractionation in river water is not as pronounced as seawater, implying that the processes and sources that give rise to this LREE-depleted pattern have been partially overprinted by dissolved REE derived from the weathering of other, siliciclastic or igneous rocks in the area (higher Pr_n/Yb_n and lower Y/Ho).

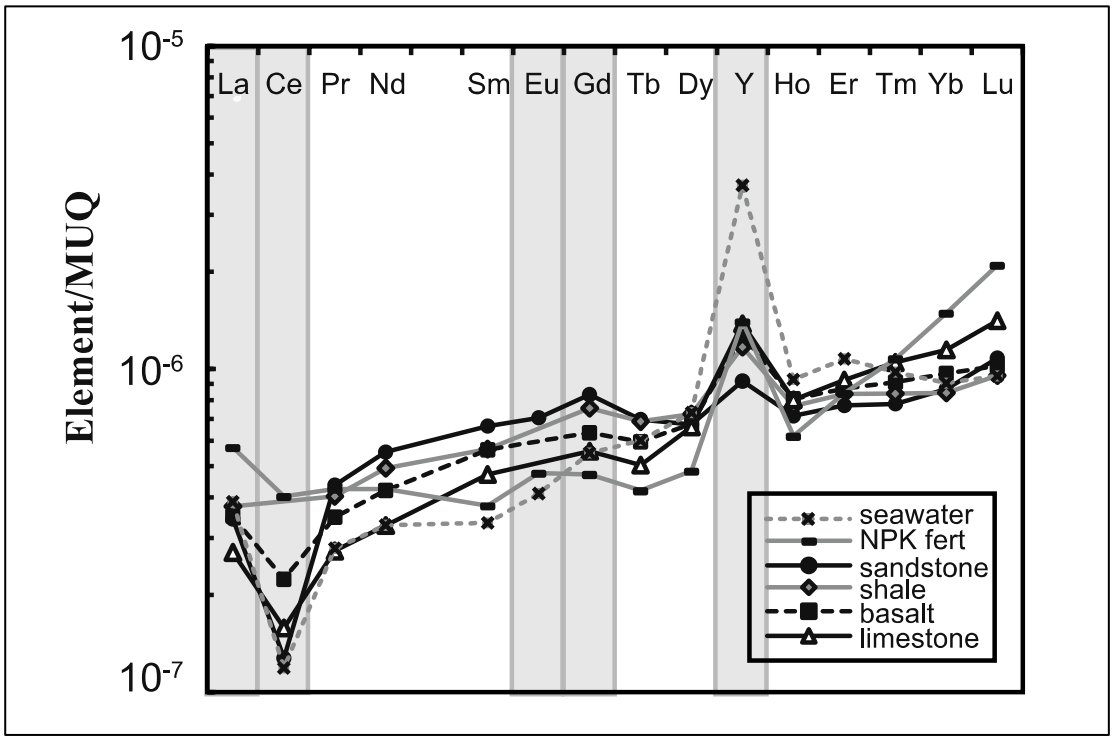

Figure 7. REE+Y distribution of streamwater. Average REE+Y pattern of NPK fertilisers (N=3) and fodder phosphate (n=1)((Hu et al., 1998) and shallow seawater REE+Y (n=12)(Alibo and Nozaki, 1999; Hongo et al., 2006) are also plotted. For visual comparison, the patterns have been scaled to a constant concentration (Lawrence et al., 2006a). Note that negative Ce and positive Y anomalies are seen in the streamwater, shallow seawater and NPK fertiliser REE+Y distribution.

The negative Ce anomaly may be more complicated in its origin since it can also reflect processes operating in soils and aqueous transport, in addition to features of the source. In general, Ce anomalies reflects the redox-induced separation of Ce^{4+} relative to remaining redox-insensitive (strictly trivalent, with the exception of Eu) LREE. This separation is well-documented to occur in soils prior to REE leaching or during aqueous transport (e.g., Wang and Liang, 2014) and previous work demonstrated that the magnitude of Ce anomalies in both groundwaters and river waters can vary as a function of topography (e.g., amount of soil-water interaction increasing downslope) and the amount and type of ligands available (Armand et al., 2015; Pourret et al., 2010). Armand et al., (2015) measured the REE concentrations of 119 streamwater samples across France and stressed that topography, residence time, wetlands and pH played key roles in the speciation of REE in river systems. With low organic carbon/Fe(Mn) ratios in the soil, a negative Ce anomaly can persist in soil solutions (Pédrot et al., 2015b). Pourret et al., (2010) found topography to be a controlling factor on the spatial distribution of Ce anomalies. Thus, as first and second order upland streams were

sampled here, these factors may have also contributed to the negative Ce anomalies, and would be consistent with the variable Ce anomalies observed in the soil leaches implying varying levels of soluble Ce available for transport into streams.

An additional factor relevant to the seawater-like REE+Y pattern of the streamwaters is the potential contribution from anthropogenic sources in the form of fertilisers with high marine phosphate composition, which is difficult to differentiate based on their similar REE pattern to seawater. The average REE pattern of NPK fertilisers (n=3) and fodder phosphate (n=1) (Hu et al., 1998), as well as shallow seawater REE (n=12) (Alibo and Nozaki, 1999; Hongo et al., 2006) are plotted with the streamwater REE from this study for the purpose of visual comparison (Fig. 7) and illustrate their overall similarity. The source and composition of the phosphate fertiliser(s) applied to this region would need to be established and without adequate contrast between those and the carbonate within the catchment, these sources cannot be discerned. However, it is noted that streamwater $^{87}Sr/^{86}Sr$ reflects differences in water-rock interactions, without an obvious evidence for a fertiliser contribution.

The distinctively seawater-like REE patterns of streamwaters are interpreted here to have most likely arisen from preferential weathering of marine carbonate sources in a complex bedrock and tillite bearing catchment that is potentially also influenced by fertiliser input, and modified from soil processes that could have changed the Ce anomaly. Importantly, despite the overall similarity of the REE+Y patterns, small variations between the streamwaters are apparent and important for coupling to the Sr isotope geochemistry.

The Sr and U concentrations ([Sr] and [U]) are two such geochemical features that discriminate the waters associated with different catchment geology, with the water in the limestone catchment and the sandstone catchment identified with the highest [Sr] and [U] and the lowest [Sr] and [U], respectively, and these features are coupled to the REE (Fig. 8d). For example, the Y/Ho is highest and the lowest Pr_n/Yb_n (steepest positive slope) are in the limestone catchment sample. This is in accordance with Moller et al., (2003) who found that waters draining dolostone and limestone have higher Y/Ho ratios with respect to igneous rocks in the study catchment in NE Italy. Here, when all samples are considered together, there are strong correlations between

[Sr] and Pr_n/Yb_n (R^2=0.87), Y/Ho (R^2=0.69) and U concentrations (R^2=0.99) in the streamwaters, some of which approach hyperbolic trends. Collectively, these trends could point to a mixing relationship between a higher Pr_n/Yb_n and lower [U] and [Sr] source and a lower Pr_n/Yb_n and higher [U] and [Sr] source, consistent with a greater contribution from the carbonate-bearing source(s) in the latter. Support for this comes from a coupling of these geochemical characteristics to $^{87}Sr/^{86}Sr$ values, discussed in section 4.5.1. The Sr isotope ratios form trends with Pr_n/Yb_n, Y/Ho, [U], and [Sr] (Fig. 8 a+c), indicating that the sandstone catchment sample approaches a broad end-member with a more radiogenic Sr isotope composition (and lower [Sr], [U], Y/Ho and flatter REE+Y pattern) and the limestone catchment sample has a less radiogenic Sr isotope composition (and higher [Sr], [U], Y/Ho and more LREE-depleted pattern). Such geochemical relationships could be explained with a silicate-hosted Sr, U, and REE+Y source being mixed with the carbonate source of these elements.

In finer scaled hydrological studies, $^{87}Sr/^{86}Sr$ and [Sr] have been successfully used to investigate rock-water interactions and water sources (e.g. Aubert et al., 2002a; Katz and Bullen, 1996; Nakano et al., 2001; Négrel et al., 2004), in some cases with REE and other trace elements (Ojiambo et al., 2003; Tricca et al., 1999) and our results further illustrate the potential of combining these tracers, however, the sampling density, applied methods, and focus of the study were not designed to more thoroughly constrain these processes. While the REE and Sr can have different aqueous characteristics and mineral sources and thus, have different capabilities as tracers, the degree of [Sr] and $^{87}Sr/^{86}Sr$ variability appears to be reflected to some extent by concomitant variability of REE+Y patterns, Y/Ho ratios and [U]. Specifically, despite the REE appearing to be dominated by carbonate/fertiliser sources, subtle variations apparently reflect small-scale differences in source with variable Sr isotope compositions that are, in part, inherited from the source bedrock.

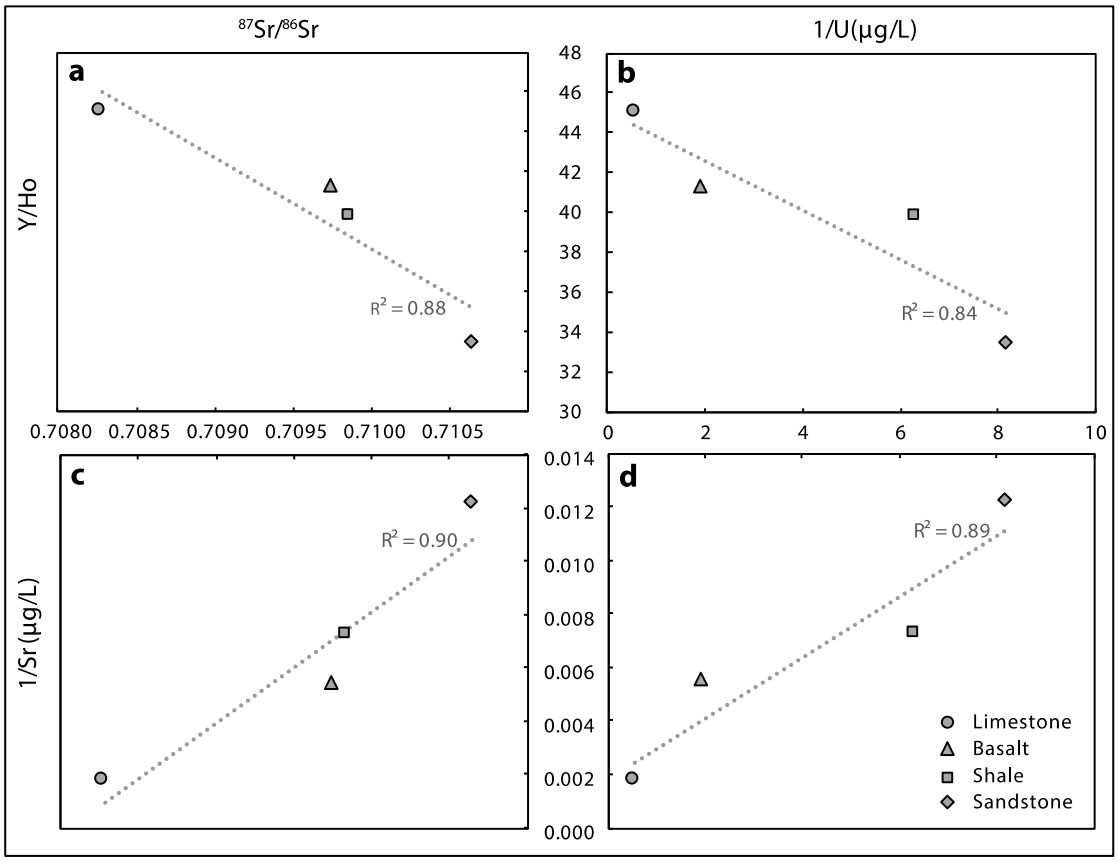

Figure 8 a. Y/Ho vs. $^{87}Sr/^{86}Sr$, **b.** Y/Ho vs. 1/U (µg/L), **c.** 1/Sr (µg/L) vs. $^{87}Sr/^{86}Sr$ and **d.** 1/Sr (µg/L) vs. 1/U (µg/L). The highly-correlated relationships between these trace elements and $^{87}Sr/^{86}Sr$ values suggest a geological control over their distribution in streamwater with water draining a limestone catchment having the highest [Sr] [U] and Y/Ho values and least radiogenic $^{87}Sr/^{86}Sr$ values. The converse is true for the streamwater draining sandstone bedrock.

5 Conclusion

This study has taken a systematic sampling approach to trace the distribution and movement of $^{87}Sr/^{86}Sr$ and trace elements, with emphasis on the REE+Y, in streamwater, soils and plants to enhance our understanding of the broad dispersal of these elements through the biosphere. The $^{87}Sr/^{86}Sr$ in streamwaters was demonstrated to have use for correlation to a specific source lithology. Streamwater REE+Y patterns have a consistent and seawater-like pattern that appears to be inherited from marine carbonate bedrock, interaction with surficial marine carbonate-derived till, anthropogenic fertiliser input or a combination of all three, but nonetheless show some variation that is coupled to the $^{87}Sr/^{86}Sr$ ratio and implies a silicate vs. carbonate source of Sr with different REE+Y characteristics that would require more samples to delineate in terms of end-member composition.

A significant fractionation phenomenon among individual REE+Y was observed during transport from the exchangeable soil to both plants and streamwater. Plants show a general tendency of decreasing transfer of REE+Y with increasing atomic mass, resulting in a LREE-enrichment. The biological absorption coefficient (BAC) of REE+Y reveals that plants from geologically discrete regions differ in absorption capacity but a striking preferential biouptake of Y is noted in all ash tree (*Fraxinus excelsior L.*) samples. The transportation of individual REE+Y in plants shows some agreement with that of the soil extracts, mostly those leached with H_2O, which captured the apparent preferential release of La, Gd, Lu, and preferential release of LREE, but overall, both NH_4NO_3 and H_2O leaches were poor indicators of REE+Y uptake in plants. Further work is necessary to understand the behaviour of the anomalous REE+Y elements in soil reservoirs (e.g., complexation, preferential release during weathering, uptake mechanisms).

The $^{87}Sr/^{86}Sr$ of soil leachates is procedurally defined and is therefore not accurately informative of the natural values that exist within the pedosphere. This finding attests to the view that plant material is most suitable for the purpose of constructing biosphere

Sr isoscapes. In contrast to some of the larger Sr biosphere mapping studies to date that have taken a more generalised regional approach, this research has spatially resolved variation at a resolution that allows for more detailed local geochemical differences to be observed. Use of discriminant analysis successfully classified certain bedrock lithologies and Quaternary deposits as isotopically coherent biosphere packages. Namely, there are significant ($p<0.05$) differences in biosphere values between sandstone/shale tills and those composed primarily of limestone. These distinguishable biosphere units demonstrate that the presence of soil-parent materials derived from both bedrock and Quaternary sediments control the $^{87}Sr/^{86}Sr$ distribution within this region. Even without a large range in $^{87}Sr/^{86}Sr$ biosphere values, significant spatial variations in $^{87}Sr/^{86}Sr$ have been characterised. Furthermore, there is sufficient $^{87}Sr/^{86}Sr$ variation within this region to give critical geographic perspective to archaeological provenance investigations.

Acknowledgments

S.E.R. was funded by a Trinity Postgraduate Studentship. C.S. was supported by the Philippe Wiener-Maurice Anspach Foundation. We thank the technical and scientific staff at University College Dublin, especially Mr. Michael Murphy, who provided invaluable help with the analyses. Nadine Mattielli, Jeroen de Jong and Wendy Debouge from the G-Time laboratory of the Université Libre de Bruxelles are also thanked for their help with strontium isotope analyses.

References

Åberg, G., Fosse, G., Stray, H., 1998. Man, nutrition and mobility: A comparison of teeth and bone from the Medieval era and the present from Pb and Sr isotopes. Sci. Total Environ. 224, 109–119.

Agnan, Y., Séjalon-Delmas, N., Probst, A., 2014. Origin and distribution of rare earth elements in various lichen and moss species over the last century in France. Sci. Total Environ. 487, 1–12.

Aide, M.T., Aide, C., 2012. Rare Earth Elements: Their Importance in Understanding Soil Genesis. ISRN Soil Sci. 2012, 1–11.

Alibo, D.S., Nozaki, Y., 1999. Rare earth elements in seawater: Particle association, shale-normalization, and Ce oxidation. Geochim. Cosmochim. Acta 63, 363–372.

Armand, R., Cherubini, C., Tuduri, J., Pastore, N., Pourret, O., 2015. Rare earth elements in French stream waters — Revisiting the geochemical continental cycle using FOREGS dataset. J. Geochemical Explor. 157, 132–142.

Aubert, D., Probst, A., Stille, P., Viville, D., 2002a. Evidence of hydrological control of Sr behavior in stream water (Strengbach catchment, Vosges mountains, France). Appl. Geochemistry 17, 285–300.

Aubert, D., Stille, P., Probst, A., 2001. REE fractionation during granite weathering and removal by waters and suspended loads: Sr and Nd isotopic evidence. Geochim. Cosmochim. Acta 65, 387–406.

Aubert, D., Stille, P., Probst, A., Gauthier-lafaye, F., Pourcelot, L., Del nero, M., 2002b. Characterization and migration of atmospheric REE in soils and surface waters. Geochim. Cosmochim. Acta 66, 3339–3350.

Babechuk, M.G., Kamber, B.S., 2011. An estimate of 1.9 Ga mantle depletion using the high-field-strength elements and Nd-Pb isotopes of ocean floor basalts, Flin Flon Belt, Canada. Precambrian Res. 189, 114–139.

Babechuk, M.G., Kamber, B.S., Greig, A., Canil, D., Kodolányi, J., 2010. The behaviour of tungsten during mantle melting revisited with implications for planetary differentiation time scales. Geochim. Cosmochim. Acta 74, 1448–1470.

Babechuk, M.G., Widdowson, M., Kamber, B.S., 2014. Quantifying chemical weathering intensity and trace element release from two contrasting basalt profiles, Deccan Traps, India. Chem. Geol. 363, 56–75.

Babechuk, M.G., Widdowson, M., Murphy, M., Kamber, B.S., 2015. A combined Y/Ho, high field strength element (HFSE) and Nd isotope perspective on basalt weathering, Deccan Traps, India. Chem. Geol. 396, 25–41.

Bailey, T.R., McArthur, J.M., Prince, H., Thirlwall, M., 2000. Dissolution methods for strontium isotope stratigraphy: Whole rock analysis. Chem. Geol. 167, 313–319.

Bain, D.C., Bacon, J.R., 1994. Strontium isotopes as indicators of mineral weathering in catchments. Catena 22, 201–214.

Bataille, C.P., Bowen, G.J., 2012. Mapping 87Sr/86Sr variations in bedrock and water for large scale provenance studies. Chem. Geol. 304–305, 39–52.

Bau, M., 1999. Scavenging of dissolved yttrium and rare earths by precipitating iron oxyhydroxide: Experimental evidence for Ce oxidation, Y-Ho fractionation, and lanthanide tetrad effect. Geochim. Cosmochim. Acta 63, 67–77.

Bau, M., Koschinsky, A., Dulski, P., Hein, J.R., 1996. Comparison of the partitioning behaviours of yttrium, rare earth elements, and titanium between hydrogenetic marine ferromanganese crusts and seawater. Geochim. Cosmochim. Acta 60, 1709–1725.

Beard, B.L., Johnson, C.M., 2000. Strontium isotope composition of skeletal material can determine the birth place and geographic mobility of humans and animals. J. Forensic Sci. 45, 1049–1061.

Bentley, R.A., 2006. Strontium Isotopes from the Earth to the Archaeological Skeleton: A Review. J. Archaeol. Method Theory 13, 135–187.

Bentley, R.A., Knipper, C., 2005. Geographical patterns in biologically available strontium, carbon and oxygen isotope signatures in prehistoric SW Germany. Archaeometry 47, 629–644.

Birck, J.L., 1986. Precision K-Rb-Sr isotopic analysis: Application to Rb-Sr chronology. Chem. Geol. 56, 73–83.

Blum, J.D., Taliaferro, E.H., Weisse, M.T., Holmes, R.T., 2000. Changes in Sr/Ca, Ba/Ca and $^{87}Sr/^{86}Sr$ ratios between trophic levels in two forest ecosystems in the northeastern U.S.A. Biogeochemistry 49, 87–101.

Bowen, G.J., Maibauer, B.J., Kraus, M.J., Röhl, U., Westerhold, T., Steimke, A., Gingerich, P.D., Wing, S.L., Clyde, W.C., 2014. Two massive, rapid releases of carbon during the onset of the Palaeocene–Eocene thermal maximum. Nat. Geosci. 8, 44–47.

Braun, J.-J., Viers, J., Dupré, B., Polvé, M., Ndam, J., Muller, J.-P., 1998. Solid/Liquid REE Fractionation in the Lateritic System of Goyoum, East Cameroon: The Implication for the Present Dynamics of the Soil Covers of the Humid Tropical Regions. Geochim. Cosmochim. Acta 62, 273–299.

Brioschi, L., Steinmann, M., Lucot, E., Pierret, M.C., Stille, P., Prunier, J., Badot, P.M., 2013. Transfer of rare earth elements (REE) from natural soil to plant systems: Implications for the environmental availability of anthropogenic REE. Plant Soil 366, 143–163.

Brooks, R.R., 1972. Geobotany and Biogeochemistry in Mineral Exploration. New York: Harper & Row.
Budd, P., Montgomery, J., Barreiro, B., Thomas, R.G., 2000. Differential diagenesis of strontium in archaeological human dental tissues. Appl. Geochemistry 15, 687–694.

Bunker, D.J., Smith, J.T., Livens, F.R., Hilton, J., 2000. Determination of radionuclide exchangeability in freshwater systems. Sci. Total Environ. 263, 171–183.

Burke, W.H., Denison, R.E., Hetherington, E. a, Koepnick, R.B., Nelson, H.F., Otto, J.B., 1982. Variation of seawater $^{87}Sr/^{86}Sr$ throughout Phanerozoic time. Geology 10, 516–519.

Byrne, R.H., Sholkovitz, E.R., 1996. Marine chemistry and geochemistry of the lanthanides., in: Gschneidner Jr., K.A., Eyring, L. (Eds.), Handbook on the Physics and Chemistry of Rare Earths. Elsevier, Amsterdam, pp. 497–593.

Cahill Wilson, J., Standish, C.D., 2016. Mobility and migration in late Iron Age and early Medieval Ireland. J. Archaeol. Sci. Reports 6, 230–241.

Capo, R.C., Stewart, B.W., Chadwick, O.A., 1998. Strontium isotopes as tracers of ecosystem processes: Theory and Methods. Geoderma 82, 197–225.

Caporale, A.G., Violante, A., 2016. Chemical Processes Affecting the Mobility of Heavy Metals and Metalloids in Soil Environments. Curr. Pollut. Reports 2, 15–27.

Censi, P., Saiano, F., Pisciotta, A., Tuzzolino, N., 2014. Geochemical behaviour of rare earths in Vitis vinifera grafted onto different rootstocks and growing on several soils. Sci. Total Environ. 473–474, 597–608.

Chudaev, O. V., Bragin, I. V., Kharitonova, N.A., Chelnokov, G.A., 2016. Distribution and Geochemistry of Rare-Earth Elements in Rivers of Southern and Eastern Primorye (Far East of Russia). IOP Conf. Ser. Earth Environ. Sci. 33.

Cidu, R., Vittori Antisari, L., Biddau, R., Buscaroli, A., Carbone, S., Da Pelo, S., Dinelli, E., Vianello, G., Zannoni, D., 2013. Dynamics of rare earth elements in water-soil systems: The case study of the Pineta San Vitale (Ravenna, Italy). Geoderma 193–194, 52–67.

Clarke, A., Parkes, M., Gatley, S., 2007. The Geological Heritage of Meath. An Audit Cty. Geol. Sites Meath. Geol. Surv. Ireland. Unpubl. Rep. 1–36.

Condie, K.C., 1991. Another look at rare earth elements in shales. Geochim. Cosmochim. Acta 55, 2527–2531.

Condie, K.C., Dengate, J., Cullers, R.L., 1995. Behavior of rare earth elements in a paleoweathering profile on granodiorite in the Front Range, Colorado, USA. Geochim. Cosmochim. Acta 59, 279–294.

Curran, J.M., Meighan, I.G., Simpson, D.D.A., Rogers, G., Fallick, A.E., 2001. $^{87}Sr/^{86}Sr$: a New Discriminant for Provenancing Neolithic Porcellanite Artifacts from Ireland. J. Archaeol. Sci. 28, 713–720.

Davies, G., Gledhill, A., Hawkesworth, C., 1985. Upper crustal recycling in southern Britain: evidence from Nd and Sr isotopes. Earth Planet. Sci. Lett. 75, 1–12.

Deberdt, S., Viers, J., Dupré, B., 2002. New insights about the rare earth elements (REE) mobility in river waters. Bull. la Société Géologique Fr. 173, 147–160.

DIN:ISO 19730, 2009. Soil quality – Extraction of trace elements from soil using ammonium nitrate solution (ISO 19730:2008), DIN, 2009.

Ding, S., Liang, T., Zhang, C., Wang, L.J., Sun, Q., 2006. Accumulation and fractionation of rare earth elements in a soil-wheat system. Pedosphere 16, 82–90.

Douthit, T.L., Meyers, W.J., Hanson, G.N., 1993. Nonmonotonic Variation of Seawater 87Sr/86Sr Across the Ivorian/Chadian Boundary (Mississippian, Osagean): Evidence from Marine Cements within the Irish Waulsortian Limestone. J. Sediment. Res. Vol. 63, 539–549.

Drouet, T., Herbauts, J., Gruber, W., Demaiffe, D., 2007. Natural strontium isotope composition as a tracer of weathering patterns and of exchangeable calcium sources in acid leached soils developed on loess of central Belgium. Eur. J. Soil Sci. 58, 302–319.

Dunn, C., 2007, Biogeochemistry in Mineral Exploration Volume 9: Elsevier, Amsterdam, 460 p.

Ebong, G.A., Etuk, H.S., Johnson, A.S., 2007. Heavy Metals Accumulation by Talinum triangulare grown on Waste Dumpsites in Uyo Metropolis, Akwa Ibom State, Nigeria. J. Appl. Sci. 7, 14.

Eggins, S.M., Woodhead, J.D., Kinsley, L.P.J., Mortimer, G.E., Sylvester, P.J., McCulloch, M.T., Hergt, J.M., Handler, M.R., 1997. A simple method for the precise determination of > 40 trace elements in geological samples by ICPMS using enriched isotope internal standardisation. Chem. Geol. 1, 311–326.

Elderfield, H., Upstill-Goddard, R., Sholkovitz, E.R., 1990. The rare earth elements in rivers, estuaries, and coastal seas and their significance to the composition of ocean waters. Geochim. Cosmochim. Acta 54, 971–991.

Ericson, J.E., 1985. Strontium isotope characterization in the study of prehistoric human ecology. J. Hum. Evol. 14, 503–514.

Evans, J.A., Chenery, C.A., Montgomery, J., 2012. A summary of strontium and oxygen isotope variation in archaeological human tooth enamel excavated from Britain. J. Anal. At. Spectrom. 27, 754.

Evans, J.A., Montgomery, J., Wildman, G., 2009. Isotope domain mapping of $^{87}Sr/^{86}Sr$ biosphere variation on the Isle of Skye, Scotland. J. Geol. Soc. London 166, 617–631.

Evans, J.A., Montgomery, J., Wildman, G., Boulton, N., 2010. Spatial variations in biosphere $^{87}Sr/^{86}Sr$ in Britain. J. Geol. Soc. London 167, 1–4.

Evans, J.A., Tatham, S., 2004. Defining “local signature” in terms of Sr isotope composition using a tenth- to twelfth-century Anglo-Saxon population living on a Jurassic clay-carbonate terrain, Rutland, UK. Geol. Soc. London, Spec. Publ.

Fang, J., Wen, B., Shan, X.Q., Wang, H. hua, Lin, J. ming, Zhang, S., 2007. Evaluation of bioavailability of light rare earth elements to wheat (Triticum aestivum L.) under field conditions. Geoderma 141, 53–59.

Faure, G., and Powell, J.L., 1972, Strontium Isotope Geology: New York, Springer-Verlag.

Fay, D., Kramers, G., and Zhang, C., 2007, Soil Geochemical Atlas of Ireland: Teagasc and Environmental Protection Agency Ireland, 120 p.

Finch, T.F., Gardiner, M., Comey, A., Radford, T., Taluntais, A.F., 1983. Soil of Co. Meath: National Soil Survey of Ireland. An Foras Taluntais.

Frei, K.M., Frei, R., 2011. The geographic distribution of strontium isotopes in Danish surface waters – A base for provenance studies in archaeology, hydrology and agriculture. Appl. Geochemistry 26, 326–340.

Frei, K.M., Frei, R., Mannering, U., Gleba, M., Nosch, M.L., Lyngstrøm, H., 2009. Provenance of Ancient Textiles-a Pilot Study Evaluating the Strontium Isotope System in Wool. Archaeometry 51, 252–276.

Frei, R., Frei, K.M., 2013. The geographic distribution of Sr isotopes from surface waters and soil extracts over the island of Bornholm (Denmark) – A base for provenance studies in archaeology and agriculture. Appl. Geochemistry 38, 147–160.

Fu, F., Akagi, T., and Shinotsuka, K., 1998, Distribution pattern of rare earth elements in fern: Biological trace element research, v. 64, P. 13-26.

Fu, F., Akagi, T., Yabuki, S., and Iwaki, M., 2001, The variation of REE (rare earth elements) patterns in soil-grown plants: A new proxy for the source of rare earth elements and silicon in plants: Plant and Soil, v. 235, p. 53–64.

Geological Survey of Ireland, 2009, Energy and Natural Resources: Bedrock Geology.

Geological Survey of Ireland, 2016, GSI Spatial Resources Viewer: Retrieved from URL: http://dcenr.maps.arcgis.com/home/webmap/viewer.html?useExisting=1.

Giero, R., Stille, P., 2004. Energy, waste and the environment -- a geochemical perspective: introduction. Geol. Soc. London, Spec. Publ. 236, 1–5.

Grimstead, D.N., Nugent, S., Whipple, J., 2017. Why a Standardization of Strontium Isotope Baseline Environmental Data Is Needed and Recommendations for Methodology. Adv. Archaeol. Pract. 1–12.

Hartman, G., Richards, M.P., 2014. Mapping and defining sources of variability in bioavailable strontium isotope ratios in the Eastern Mediterranean. Geochim. Cosmochim. Acta 126, 250–264.

Hedman, K.M., Curry, B.B., Johnson, T.M., Fullagar, P.D., Emerson, T.E., 2009. Variation in strontium isotope ratios of archaeological fauna in the Midwestern United States: a preliminary study. J. Archaeol. Sci. 36, 64–73.

Hendry, J.P., Gregg, J.M., Shelton, K.L., Somerville, I.D., Crowley, S.F., 2015. Origin, characteristics and distribution of fault-related and fracture-related dolomitization: Insights from Mississippian carbonates, Isle of Man. Sedimentology 62, 717–752.

Hodell, D., Quinn, R.L., Brenner, M., Kamenov, G., 2004. Spatial variation of strontium isotopes ($^{87}Sr/^{86}Sr$) in the Maya region: a tool for tracking ancient human migration. J. Archaeol. Sci. 31, 585–601.

Hongo, Y., Obata, H., Alibo, D.S., Nozaki, Y., 2006. Spatial Variations of Rare Earth Elements in North Pacific Surface Water. J. Oceanogr. 62, 441–455.

Horwitz, E.P., Chiarizia, R., Dietz, M.L., 1992. A Novel Strontium-Selective Extraction Chromatographic Resin*. Solvent Extr. Ion Exch. 10, 313–336.

Hu, Y., Vanhaecke, F., Moens, L., Dams, R., Del Castilho, P., Japenga, J., 1998. Determination of the aqua regia soluble content of rare earth elements in fertilizer, animal fodder phosphate and manure samples using inductively coupled plasma mass spectrometry. Anal. Chim. Acta 373, 95–105.

Hu, Z., Haneklaus, S., Sparovek, G., Schnug, E., 2006. Rare Earth Elements in Soils. Commun. Soil Sci. Plant Anal. 37, 1381–1420.

Huang, C.M., Gong, Z.T., 2001. Geochemical implication of rare earth elements in process of soil development. J. Rare Earths 19, 57–62.

Johannesson, K.H., Farnham, I.M., Guo, C., Stetzenbach, K.J., 1999. Rare earth element fractionation and concentration variations along a groundwater flow path within a shallow, basin-fill aquifer, southern Nevada, USA. Geochim. Cosmochim. Acta 63, 2697–2708.

Johannesson, K.H., Hawkins, D.L., Cortés, A., 2006. Do Archean chemical sediments record ancient seawater rare earth element patterns? Geochim. Cosmochim. Acta 70, 871–890.

Johannesson, K.H., Hendry, M.J., 2000. Rare earth element geochemistry of groundwaters from a thick till and clay-rich aquitard sequence, Saskatchewan, Canada. Geochim. Cosmochim. Acta 64, 1493–1509.

Johannesson, K.H., Lyons, W.B., 1994. The rare earth element geochemistry of Mono Lake water and the importance of carbonate complexing. Limnol. Oceanogr. 39, 1141–1154.

Johannesson, K.H., Zhou, X., 1999. Origin of middle rare earth element enrichments in acid waters of a Canadian High Arctic lake. Geochim. Cosmochim. Acta 63, 153–165.

Johnson, C., Breward, N., Ander, E.L., Ault, L., 2005. G-BASE: baseline geochemical mapping of Great Britain and Northern Ireland. Geochemistry Explor. Environ. Anal. 5, 347–357.

Kabata-Pendias, A., 2001, Trace elements in soils and plants: CRC Press; Boca Raton; London, 3rd Edition, 331 p.

Kador, T., Fibiger, L., Cooney, G., and Fullagard, P., 2014, Movement and diet in early Irish prehistory: first evidence from multi-isotope analysis: The Journal of Irish Archaeology. XXIII, 83–96.

Kamber, B.S., Greig, A., Collerson, K.D., 2005. A new estimate for the composition of weathered young upper continental crust from alluvial sediments, Queensland, Australia. Geochim. Cosmochim. Acta 69, 1041–1058.

Kamber, B.S., Webb, G.E., Gallagher, M., 2014. The rare earth element signal in Archaean microbial carbonate: information on ocean redox and biogenicity 171, 745–763.

Kastori, R.R., Maksimović, I. V., Zeremski-Škorić, T.M., Putnik-Delić, M.I., 2010. Rare earth elements: Yttrium and higher plants. Zb. Matice Srp. za Prir. Nauk. 87–98.

Katz, B.G., Bullen, T.D., 1996. The combined use of $^{87}Sr/^{86}Sr$ and carbon and water isotopes to study the hydrochemical interaction between groundwater and lakewater in mantled karst. Geochim. Cosmochim. Acta 60, 5075–5087.

Khan, A.M., Behkami, S., Yusoff, I., Md Zain, S. Bin, Bakar, N.K.A., Bakar, A.F.A., Alias, Y., 2017. Geochemical characteristics of rare earth elements in different types of soil: A chemometric approach. Chemosphere 184, 673–678.

Knudson, K.J., O'Donnabhain, B., Carver, C., Cleland, R., Price, T.D., 2012. Migration and Viking Dublin: Paleomobility and paleodiet through isotopic analyses. J. Archaeol. Sci. 39, 308–320.

Knudson, K.J., Torres-Rouff, C., 2009. Investigating cultural heterogeneity in san pedro de atacama, northern chile, through biogeochemistry and bioarchaeology. Am. J. Phys. Anthropol. 138, 473–485.

Kootker, L.M., van Lanen, R.J., Kars, H., Davies, G.R., 2016. Strontium isoscapes in The Netherlands. Spatial variations in 87Sr/86Sr as a proxy for palaeomobility. J. Archaeol. Sci. Reports 6, 1–13.

Laffoon, J.E., 2012, Patterns of paleomobility in the ancient Antilles: an isotopic approach: Ph.D. Thesis. Leiden University.

Laffoon, J.E., Davies, G.R., Hoogland, M.L.P., Hofman, C.L., 2012. Spatial variation of biologically available strontium isotopes ($^{87}Sr/^{86}Sr$) in an archipelagic setting: a case study from the Caribbean. J. Archaeol. Sci.

Laffoon, J.E., Sonnemann, T.F., Shafie, T., Hofman, C.L., Brandes, U., Davies, G.R., 2017. Investigating human geographic origins using dual-isotope ($^{87}Sr/^{86}Sr$, ^{18}O) assignment approaches. PLoS One 12, 1–16.

Lagad, R.A., Singh, S.K., Rai, V.K., 2017. Rare earth elements and $^{87}Sr/^{86}Sr$ isotopic characterization of Indian Basmati rice as potential tool for its geographical authenticity. Food Chem. 217, 254–265.

Laul, J.C., Weimer, W.C., Rancitelli, L.A., 1979. Biogeochemical distribution of rare earths and other trace elements in plants and soils. Phys. Chem. Earth 11, 819–827.

Laveuf, C., Cornu, S., 2009. A review on the potentiality of Rare Earth Elements to trace pedogenetic processes. Geoderma 154, 1–12.

Lawrence, M.G., Greig, A., Collerson, K.D., Kamber, B.S., 2006a. Rare earth element and yttrium variability in South East Queensland waterways. Aquat. Geochemistry 12, 39–72.

Lawrence, M.G., Jupiter, S.D., Kamber, B.S., 2006b. Aquatic geochemistry of the rare earth elements and yttrium in the Pioneer River catchment, Australia. Mar. Freshw. Res. 57, 725–736.

Lawrence, M.G., Kamber, B.S., 2006. The behaviour of the rare earth elements during estuarine mixing-revisited. Mar. Chem. 100, 147–161.

Leybourne, M.I., Goodfellow, W.D., Boyle, D.R., Hall, G.M., 2000. Rapid development of negative Ce anomalies in surface waters and contrasting REE patterns in groundwaters associated with Zn-Pb massive sulphide deposits. Appl. Geochemistry 15, 695–723 15.

Leybourne, M.I., Johannesson, K.H., 2008. Rare earth elements (REE) and yttrium in stream waters, stream sediments, and Fe–Mn oxyhydroxides: Fractionation, speciation, and controls over REE + Y patterns in the surface environment. Geochim. Cosmochim. Acta 72, 5962–5983.

Lima e Cunha, M. do C., Nardi, L.V.S., Pereira, V.P., Bastos Neto, A.C., Vedana, L.A., 2014. Evaluation of Biological Absorption Coefficient of Trace Elements in Plants From the Pitinga Mine District, Amazonian Region. Rev. do Inst. Geológico 35, 19–29.

Loell, M., Reiher, W., Felix-Henningsen, P., 2011. Contents and bioavailability of rare earth elements in agricultural soils in Hesse (Germany). J. Plant Nutr. Soil Sci. 174, 644–654.

Ma, L., Jin, L., Brantley, S.L., 2011. How mineralogy and slope aspect affect REE release and fractionation during shale weathering in the Susquehanna/Shale Hills Critical Zone Observatory. Chem. Geol. 290, 31–49.

Matsunaga, T., Tsuduki, K., Yanase, N., Kritsananuwat, R., Hanzawa, Y., Naganawa, H., 2015. Increase in rare earth element concentrations controlled by dissolved organic matter in river water during rainfall events in a temperate, small forested catchment. J. Nucl. Sci. Technol. 52, 514–529.

Maurer, A.-F., Galer, S.J.G., Knipper, C., Beierlein, L., Nunn, E. V, Peters, D., Tütken, T., Alt, K.W., Schöne, B.R., 2012. Bioavailable $^{87}Sr/^{86}Sr$ in different environmental samples - Effects of anthropogenic contamination and implications for isoscapes in past migration studies. Sci. Total Environ. 433, 216–29.

McArthur, J.M., Howarth, R., Bailey, T., 2001. Strontium isotope stratigraphy: LOWESS version 3: Best fit to the marine Sr-isotope curve for 0–509 Ma and accompanying look-up table for deriving. J. Geol. 109, 155–170.

McCabe, M., 2007. Glacial Geology and Geomorphology. The Landscapes of Ireland. Dunedin, Edinburgh.

McConnell, B., Philcox, M.E., and Geraghty, M., 2001, Geology Of Meath. A Geological Description To Accompany The Bedrock Geology 1:100,000 Scale Map Sheet 13, Meath: Department of Public Enterprise.

Meehan, R.T., and Warren, W.P., 1999, The Boyne Valley in the Ice Age: A field guide to some of the valley's most important glacial geological features: Meath County Council and the Geological Survey of Ireland. 84 p.

Miao, L., Ma, Y., Xu, R., Yan, W., 2011. Environmental biogeochemical characteristics of rare earth elements in soil and soil-grown plants of the Hetai goldfield, Guangdong Province, China. Environ. Earth Sci. 63, 501–511.

Miao, L., Xu, R., Ma, Y., Zhu, Z., Wang, J., Cai, R., Chen, Y., 2008. Geochemistry and biogeochemistry of rare earth elements in a surface environment (soil and plant) in South China. Environ. Geol. 56, 225–235.

Miekeley, N., Casartelli, E.A., Dotto, R.M., 1994. Concentration levels of rare-earth elements and thorium in plants from the Morro do Ferro environment as an indicator for the biological availability of transuranium elements. J. Radioanal. Nucl. Chem. Artic. 182, 75–89.

Miller, E., Blum, J.D., Friedland, A., 1993. Determination of soil exchangeable-cation loss and weathering rates using Sr isotopes. Nature 362, 438–441.

Millero, F.J., 1992. Stability constants for the formation of rare earth-inorganic complexes as a function of ionic strength. Geochim. Cosmochim. Acta 56, 3123–3132.

Möller, P., Morteani, G., Dulski, P., 2003. Anomalous Gadolinium, Cerium, and Yttrium contents in the Adige and Isarco River waters and in the water of their tributaries (Provinces Trento and Bolzano/Bozen, NE Italy). Acta Hydrochim. Hydrobiol. 31, 225–239.

Montgomery, J., 2010. Passports from the past: Investigating human dispersals using strontium isotope analysis of tooth enamel. Ann. Hum. Biol. 37, 325–46.

Montgomery, J., Evans, J.A., Chenery, C.A., 2006a. Report of the lead, strontium, and oxygen isotope analysis of the Iron Age burial from Rath, Ireland. Unpubl. Rep. CRDS Ltd, Dublin, Ireland. 13 pp.

Montgomery, J., Evans, J.A., Cooper, R.E., 2007. Resolving archaeological populations with Sr-isotope mixing models. Appl. Geochemistry 22, 1502–1514.

Montgomery, J., Evans, J.A., Neighbour, T., 2003. Sr isotope evidence for population movement within the Hebridean Norse community of NW Scotland. J. Geol. Soc. London. 160, 649–653.

Montgomery, J., Evans, J.A., Wildman, G., 2006b. $^{87}Sr/^{86}Sr$ isotope composition of bottled British mineral waters for environmental and forensic purposes. Appl. Geochemistry 21, 1626–1634.

Montgomery, J., and Grimes, V., 2010, Appendix 21.1: Report on the isotope analysis of a burial from Ratoath, Co. Meath., in C. Corlett and M. Potterton (Eds.). Death and Burial in Early Medieval Ireland in the Light of Recent Archaeological Excavations. Wordwell, Dublin, Ireland, pp. 309–311.

Montgomery, J., Grimes, V., Buckberry, J., Evans, J.A., Richards, M.P., Barrett, J.H., 2014. Finding Vikings with isotope analysis: The view from wet and windy islands. J. North Atl. 7, 54–70.

Nafplioti, A., 2011. Tracing population mobility in the Aegean using isotope geochemistry: a first map of local biologically available $^{87}Sr/^{86}Sr$ signatures. J. Archaeol. Sci. 38, 1560–1570.

Nakano, T., Yokoo, Y., Yamanaka, M., 2001. Strontium isotope constraint on the provenance of basic cations in soil water and stream water in the Kawakami volcanic watershed, central Japan. Hydrol. Process. 15, 1859–1875.

Négrel, P., Guerrot, C., Cocherie, A., Azaroual, M., Brach, M., Fouillac, C., 2000. Rare earth elements, neodymium and strontium isotopic systematics in mineral waters: evidence from the Massif Central, France. Appl. Geochemistry 15, 1345–1367.

Négrel, P., Giraud, E.P., Widory, D., 2004. Strontium isotope geochemistry of alluvial groundwater: a tracer for groundwater resources characterisation. Hydrol. Earth Syst. Sci. Discuss. 8, 959–972.

Négrel, P., Guerrot, C., Millot, R., 2007. Chemical and strontium isotope characterization of rainwater in France: influence of sources and hydrogeochemical implications. Isotopes Environ. Health Stud. 43, 179–196.

Nesbitt, H., 1979. Mobility and fractionation of REE during wearhering of a granodiorite. Nature 279, 206–210.

Noack, C.W., Dzombak, D.A., Karamalidis, A.K., 2014. Rare earth element distributions and trends in natural waters with a focus on groundwater. Environ. Sci. Technol. 48, 4317–4326.

Ojiambo, S.B., Lyons, W.B., Welch, K.A., Poreda, R.J., Johannesson, K.H., 2003. Strontium isotopes and rare earth elements as tracers of groundwater-lake water interactions, Lake Naivasha, Kenya. Appl. Geochemistry 18, 1789–1805.

O'Connor, P.J., 1988, Strontium isotope geochemistry of Tertiary igneous rocks, NE Ireland, in A.C. Morton and L.M. Parson (Eds.), Early Tertiary Volcanism, Geological Society Special Publication No. 39, pp. 361–363.

Pack, A., Russell, S.S., Shelley, J.M.G., van Zuilen, M., 2007. Geo- and cosmochemistry of the twin elements yttrium and holmium. Geochim. Cosmochim. Acta 71, 4592–4608.

Pearcy, R., Ehleringer, J., Mooney, H.A., and Rundel, P.W. (Eds.), 2000, Plant Physiological Ecology: Field methods and instrumentation: Kluwer Academic Publishers. 80, pp. 1-1785.

Pédrot, M., Dia, A., Davranche, M., Gruau, G., 2015a. Upper soil horizons control the rare earth element patterns in shallow groundwater. Geoderma 239, 84–96.

Pédrot, M., Dia, A., Davranche, M., Gruau, G., 2015b. Upper soil horizons control the rare earth element patterns in shallow groundwater. Geoderma 239, 84–96.

Pierson-Wickmann, A.C., Aquilina, L., Weyer, C., Molénat, J., Lischeid, G., 2009. Acidification processes and soil leaching influenced by agricultural practices revealed by strontium isotopic ratios. Geochim. Cosmochim. Acta 73, 4688–4704.

Piper, D.Z., Bau, M., 2013. Normalized Rare Earth Elements in Water, Sediments, and Wine : Identifying Sources and Environmental Redox Conditions. Am. J. Anal. Chem. 2013, 69–83.

Porder, S., Paytan, A., and Hadly, E.A., 2003, Mapping the origin of faunal assemblages using strontium isotopes: Paleobiology. 29, 197–204.

Poszwa, A., Dambrine, E., Ferry, B., Pollier, B., Loubet, M., 2002. Do deep tree roots provide nutrients to the tropical rainforest? Biogeochemistry 60, 97–118.

Poszwa, A., Dambrine, E., Pollier, B., Atteia, O., 2000. A comparison between Ca and Sr cycling in forest ecosystems. Plant Soil 225, 299–310.

Pourret, O., Gruau, G., Dia, A., Davranche, M., Molénat, J., 2010. Colloidal control on the distribution of rare earth elements in shallow groundwaters. Aquat. Geochemistry 16, 31–59.

Price, T.D., 2015. An Introduction to the Isotopic Studies of Ancient Human Remains. J. North Atl. 7, 71–87.

Price, T.D., Burton, J.H., Sharer, R.J., Buikstra, J.E., Wright, L.E., Traxler, L.P., Miller, K.A., 2010. Kings and commoners at Copan: Isotopic evidence for origins and movement in the Classic Maya period. J. Anthropol. Archaeol. 29, 15–32.

Price, T.D., Frei, K.M., Naumann, E., 2014. Isotopic Baselines in the North Atlantic Region. J. North Atl. 7, 103–136.

Price, T.D., Naumann, E., 2015. The Peopling of the North Atlantic: Isotopic Results from Norway. J. North Atl. 7, 88–102.

Robinson, W.O., Bastron, H., Murata, K.J., 1958. Biogeochemistry of the rare-earth elements with particular reference to hickory trees. Geochim. Cosmochim. Acta 14, 55–67.

Rust, S., Savill, P.S., 2000. The root systems of Fraxinus excelsior and Fagus sylvatica and their competitive relationships. Forestry 73, 499–508.

Sadeghi, M., Morris, G.A., Carranza, E.J.M., Ladenberger, A., Andersson, M., 2013. Rare earth element distribution and mineralization in Sweden: An application of principal component analysis to FOREGS soil geochemistry. J. Geochemical Explor. 133, 160–175.

Sahai, N., Carroll, S.A., Rocberts, S., O'Day, P.A., 2000. X-Ray Absorption Spectroscopy of Strontium(II) Coordination. J. Colloid Interface Sci. 222, 184–197.

Sealy, J.C., van der Merwe, N.J., Sillen, A., Kruger, F.J., Krueger, H.W., 1991. $^{87}Sr/^{86}Sr$ as a dietary indicator in modern and archaeological bone. J. Archaeol. Sci. 18, 399–416.

Shacklette, H.T., Boerngen, J.G., 1984. Element concentrations in soils and other surfical materials of the conterminous United States. U.S. Geol. Surv. Prof. Pap. 1270 1–63.

Sheridan, J.A., Jay, M., Montgomery, J., Pellegrini, M., and Cahill Wilson, J., 2013, "Tara Boy": local hero or international man of mystery?, in M. O' Sullivan, M. Doyle and C. Scarre (Eds.), Tara-from the past to the future, Wordwell: Dublin.

Sholkovitz, E.R., 1995. The aquatic chemistry of rare earth elements in rivers and estuaries. Aquat. Geochemistry 1, 1–34.

Sholkovitz, E.R., Landing, W.M., Lewis, B.L., 1994. Ocean particle chemistry: The fractionation of rare earth elements between suspended particles and seawater. Geochim. Cosmochim. Acta 58, 1567–1579.

Sillen, A., Kavanagh, M., 1982. Strontium and paleodietary research: A review. Am. J. Phys. Anthropol. 25, 67–90.

Sjögren, K.G., Price, T.D., Ahlström, T., 2009. Megaliths and mobility in south-western Sweden. Investigating relationships between a local society and its neighbours using strontium isotopes. J. Anthropol. Archaeol. 28, 85–101.

Smedley, P.L., 1991. The geochemistry of rare earth elements in groundwater from the Carnmenellis area, southwest England. Geochim. Cosmochim. Acta 55, 2767–2779 7.

Smyth, D., 2007, Methods used in the Tellus Geochemical Mapping of Northern Ireland, in British Geological Survey Open Report, OR/07/022. 1–89.

Snoeck, C., Lee-Thorp, J.A., Schulting, R.J., de Jong, J., Debouge, W., Mattielli, N., 2015. Calcined bone provides a reliable substrate for strontium isotope ratios as shown by an enrichment experiment. Rapid Commun. Mass Spectrom. 29, 107–114.

Snoeck, C., Pouncett, J., Ramsey, G., Meighan, I.G., Mattielli, N., Goderis, S., Lee-Thorp, J.A., Schulting, R.J., 2016. Mobility during the Neolithic and Bronze Age in Northern Ireland explored using strontium isotope analysis of cremated human bone. Am. J. Phys. Anthropol. 160, 397–413.

Squadrone, S., Brizio, P., Battuello, M., Nurra, N., Sartor, R.M., Benedetto, A., Pessani, D., Abete, M.C., 2017. A first report of rare earth elements in northwestern Mediterranean seaweeds. Mar. Pollut. Bull. 122, 236–242.

Stille, P., Steinmann, M., Pierret, M.C., Gauthier-Lafaye, F., Aubert, D., Probst, A., Viville, D., Chabaux, F., 2006. The impact of vegetation on fractionation of rare earth elements (REE) during water-rock interaction. J. Geochemical Explor. 88, 341–344.

Taylor, S.R., McLennan, S., 1985. The continental crust: Its composition and evolution. McClennan, Blackwell Sci. Publ. 21, 85–86.

Thomas, P.J., Carpenter, D., Boutin, C., Allison, J.E., 2014. Rare earth elements (REEs): Effects on germination and growth of selected crop and native plant species. Chemosphere 96, 57–66.

Thompson, A., Amistadi, M.K., Chadwick, O.A., Chorover, J., 2013. Fractionation of yttrium and holmium during basaltic soil weathering. Geochim. Cosmochim. Acta 119, 18–30.

Thornton, E.K., 2011. Reconstructing ancient Maya animal trade through strontium isotope ($^{87}Sr/^{86}Sr$) analysis. J. Archaeol. Sci. 38, 3254–3263.

Tricca, A., Stille, P., Steinmann, M., Kiefel, B., Samuel, J., Eikenberg, J., 1999. Rare earth elements and Sr and Nd isotopic compositions of dissolved and suspended loads from small river systems in the Vosges mountains (France), the river Rhine and groundwater. Chem. Geol. 160, 139–158.

Tweed, S.O., Weaver, T.R., Cartwright, I., Schaefer, B., 2006. Behavior of rare earth elements in groundwater during flow and mixing in fractured rock aquifers: An example from the Dandenong Ranges, southeast Australia. Chem. Geol. 234, 291–307.

Tyler, G., 2004. Rare earth elements in soil and plant systems - A review. Plant Soil 267, 191–206.

Tyler, G., Olsson, T., 2005. Rare earth elements in forest-floor herbs as related to soil conditions and mineral nutrition. Biol. Trace Elem. Res. 106, 177–191.

U.S. EPA, 1996, Method 1669 Sampling Ambient Water for Trace Metals at EPA Water Quality Criteria Levels: U.S. Environmental Protection Agency.

Vázquez Vázquez, F.A., Pérez Cid, B., Río Segade, S., 2016. Assessment of metal bioavailability in the vineyard soil-grapevine system using different extraction methods. Food Chem. 208, 199–208.

Vinciguerra, V., Stevenson, R., Pedneault, K., Poirier, A., Hélie, J.F., Widory, D., 2016. Strontium isotope characterization of wines from Quebec, Canada. Food Chem. 210, 121–128.

Voerkelius, S., Lorenz, G.D., Rummel, S., Quétel, C.R., Heiss, G., Baxter, M., Brach-Papa, C., Deters-Itzelsberger, P., Hoelzl, S., Hoogewerff, J., Ponzevera, E., Van Bocxstaele, M., Ueckermann, H., 2010. Strontium isotopic signatures of natural mineral waters, the reference to a simple geological map and its potential for authentication of food. Food Chem. 118, 933–940.

Wallace, A., Montgomery, J., Grimes, V., 2010. Excavation of an Early Medieval cemetery at Ratoath, Co. Meath., in: In C. Corlett & M. Potterton (Eds.) Death and Burial in Early Medieval Ireland in the Light of Recent Archaeological Excavations. Bray: Wordwell, pp. 335–359.

Wallace, J., Ellam, R.M., Meighan, I.G., 1994. Sr isotope data for the Tertiary lavas of Northern Ireland: evidence for open system petrogenesis. J. Geol. Soc. London 151, 869–877.

Wang, L., Liang, T., 2014. Geochemical fractions of rare earth elements in atmospheric particulates around a mine tailing in Baotou, China. Atmos. Environ. 88, 23–29.

Warham, J.O., 2012. Mapping biosphere strontium isotope ratios across major lithological boundaries. PhD Thesis. University of Bradford.

Wei, Z., Yin, M., Zhang, X., Hong, F., Li, B., Tao, Y., Zhao, G., Yan, C., 2001. Rare earth elements in naturally grown fern Dicranopteris linearis in relation to their variation in soils in South-Jiangxi region (Southern China). Environ. Pollut. 114, 345–355.

Weis, D., Kieffer, B., Maerschalk, C., Barling, J., de Jong, J., Williams, G.A., Hanano, D., Pretorius, W., Mattielli, N., Scoates, J.S., Goolaerts, A., Friedman, R.M., Mahoney, J.B., 2006. High-precision isotopic characterization of USGS reference materials by TIMS and MC-ICP-MS. Geochemistry, Geophys. Geosystems 7, 1–30.

Wen, B., Yuan, D.A., Shan, X.Q., Li, F.L., Zhang, S.-Z., 2001. The influence of rare earth element fertilizer application on the distribution and bioaccumulation of rare earth elements in plants under field conditions. Chem. Speciat. Bioavailab. 13, 39–48.

Wiche, O., Zertani, V., Hentschel, W., Achtziger, R., Midula, P., 2017. Germanium and rare earth elements in topsoil and soil-grown plants on different land use types in the mining area of Freiberg (Germany). J. Geochemical Explor. 175, 120–129.

Willmes, M., Mcmorrow, L., Kinsley, L., Armstrong, R.A., Aubert, M., Eggins, S., Falgueres, C., Maureille, B., Moffat, I., Grun, R., 2014. The IRHUM (Isotopic Reconstruction of Human Migration)

database - bioavailable strontium isotope ratios for geochemical fingerprinting in France. Earth Syst. Sci. Data 6, 117–122.

Wyttenbach, A., Furrer, V., Schleppi, P., Tobler, L., 1998. Rare earth elements in soil and in soil-grown plants. Plant Soil 199, 267–273.

Xu, Z., Han, G., 2009. Chemical and strontium isotope characterization of rainwater in Beijing, China. Atmos. Environ. 43, 1954–1961.

Young, M.E., Donald, A.W., 2013. A guide to the Tellus data. Geological Survey of Northern Ireland, Belfast.

Young, M.E., Knights, K., Smyth, D., Scanlon, R., Gallagher, V., 2016. The Tellus geochemical surveys, results and applications, in: Young, M. (Ed.), Unearthed: Impacts of the Tellus Surveys of the North of Ireland. Royal Irish Academy, pp. 33–52.

Yu, K.-F., Kamber, B.S., Lawrence, M.G., Greig, A., Zhao, J.-X., 2007. High-precision analysis on annual variations of heavy metals, lead isotopes and rare earth elements in mangrove tree rings by inductively coupled plasma mass spectrometry. Nucl. Instruments Methods Phys. Res. Sect. B Beam Interact. with Mater. Atoms 255, 399–408.

Zhai, H., Yang, Y., Zheng, S., Hu, A., Zhang, S., Wang, L., 1999. Selection of the extractants for available rare earths in soils. China Environ. Sci. 67–71.

Zhang, X.C., Nearing, M. a., Polyakov, V.O., Friedrich, J.M., 2003. Using Rare-Earth Oxide Tracers for Studying Soil Erosion Dynamics. Soil Sci. Soc. Am. J. 67, 279.

Zitek, A., Tchaikovsky, A., Irrgeher, J., Waidbacher, H., Prohaska, T., 2015. The $^{87}Sr/^{86}Sr$ river water isoscape of the Danube catchment, in: Igor Liška, Franz Wagner, Manfred Sengl, K.D. and J.S. (Ed.), Joint Danube Survey 3: A Comprehensive Analysis of Danube Water Quality. ICPDR - International Commission for the Protection of the Danube River, pp. 349–354.